Qualcomm Technologies, Inc.

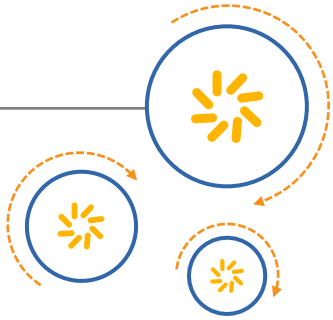

LTE Unmanned Aircraft Systems

Trial Report

v1.0.1

May 12, 2017

Qualcomm Technologies, Inc.
5775 Morehouse Drive
San Diego, CA 92121
U.S.A.

Revision history

Revision	Date	Description
1.0.0	May 2, 2017	Initial release
1.0.1	May 12, 2017	Correction to equation (2-4)

Contents

Figures

Tables

1 Introduction

This document presents initial findings from the LTE Unmanned Aircraft Systems (UAS) trial performed by Qualcomm Technologies, Inc. (QTI).

Our goal is to provide information that enhances understanding of the applicability and performance of ground-based cellular networks for providing connectivity to low-altitude drones.

To this goal, data was collected during flights at our UAS Flight Center, processed, and analyzed (field trials). Further, simulations were performed by QTI to enable analysis of characteristics not available in the current flight tests (simulations).

Field trials

The purpose of the field trials is to collect an array of data logs during flights in an operational commercial LTE network to enable quantitative analysis of performance characteristics along several dimensions, as explained in this document.

Flights were performed at a range of altitudes and using communications in three different LTE bands supported by a commercial LTE network to enable direct comparisons. These flights are complemented by ground drive routes with (nearly) the same pattern as the flight tests to facilitate comparisons with ground conditions.

Simulations

Simulations complement field trial results by allowing study of performance tradeoffs when the network is serving many ground and airborne UEs (drones) simultaneously over a wide area. Simulations also enable rapid testing of parameter and feature changes that are more difficult to study in an operational commercial network.

Simulations in this trial were performed to:

- Quantify downlink (DL) signal to interference plus noise ratio (SINR) distribution
- Study the impact of uplink (UL) power control design on network interference
- Quantify handover performance differences between ground and airborne UEs

1.1 Executive summary

This document presents results of the first comprehensive, systematic study of cellular system performance in networks serving low-altitude (120 meters above ground level and below) airborne UEs (drones) known at time of publication.

During the field trial, hundreds of flights were performed to:

- Validate the safety of the flight platform
- Validate the completeness and correctness of the logged data
- Collect the data sets for final analysis

Final data sets used to perform statistical analysis for evaluating performance were trimmed to 45 flights across a range of altitudes and focused on three cellular bands: PCS, AWS, and 700 MHz.

The data from these flights was clipped in time to include only data collected while the drone was at the intended altitude and moving at the intended speed, preventing data collected before launch and during altitude transitions from impacting and skewing the statistical results.

Field data analysis is complemented with system simulations intended to expand understanding beyond performance of a single drone in the network, and to enable study of features and configurations that are more difficult to study in an operational commercial network.

The focus of the simulations is to predict downlink SINR distributions, and to study the impact of power control and resource partitioning enhancements on uplink interference and throughputs as the number of drones in the network grows.

1.1.1 Key results

- Received signal strengths for UEs at altitude are strong despite downtilted antennas in the network. In fact, strengths are statistically stronger for UEs at altitude than for ground UEs because the free space propagation conditions at altitude more than make up for antenna gain reductions. See Figure 2-8.
- Downlink SINRs are statistically lower for UEs at altitude than for ground UEs (median decrease of 5 dB) due to neighbor cell interference. However, the coverage outage probability (defined as SINR < -6 dB) is similar for airborne and ground users, at approximately 1%. Given the downlink data rates required for drone use cases are mostly limited (for example, command and control), commercial LTE networks should be able to support downlink communications requirements of initial LTE connected drone deployment without any change. See Figure 3-1.
- For uplink communications, UE transmit power is lower at altitude than ground UEs; see Figure 2-13. However, UEs at altitude produce more uplink interference in the network than ground UEs because free space propagation increases the interference energy received at neighbor cells; see Figure 2-14. With the UE and network configurations present during field data collection, UEs at altitude produced approximately 3x the interference as a ground UE in 700 MHz band. This effect should not be an issue for initial deployment of LTE connected drones with some of them supporting high-bandwidth uplink transmission.
- Optimizations in power control are shown in simulations to mitigate excess uplink interference effectively. For example, the interference issue is eliminated in simulations with the *Optimized OLPC* approach that not only sets target signal strength at the serving cell, but also limits neighbor cell interference using downlink path loss estimation. Thus, many more drone UEs with high uplink data rate can be supported without causing excessive interference to the network or severe degradation to ground UE throughputs. See Section 3.4.1. This algorithm is attractive because it does not require the network to identify airborne UEs to be treated differently in power control. Implementing these optimizations would allow LTE

networks to better support wide scale deployments of connected drones with high-bandwidth uplink transmission (e.g., high-resolution video feeding).

- Handover performance (success rate of handovers, and lower frequency of handover events) is superior for airborne UEs than for ground UEs. This is attributed to the increased stability of signals with free space propagation relative to those subjected to the multipath, shadowing, and clutter experienced on the ground; see Section 3.5.1. However, handover algorithm can be further optimized to better support airborne UE mobility performance.

NOTE: The conclusions and results shown here are subject to the limitations of this study. It was important to construct a consistent flight path that could be executed repeatedly at different altitudes to enable apples-to-apples comparisons of results. However this flight path does not exhaustively cover all conditions. For example, the path was chosen to give us diversity of serving cells so we could study handover events and interference at cell edges. Thus, we did not fly directly over any cells where the signal strengths would be expected to be even higher than those reported here. Also, the environment was a suburban residential/commercial area with good cellular network coverage in the bands studied and these results may not directly extend to urban or rural environments with different coverage and propagation characteristics. Further, simulation results can only approximate performance of a deployed and operation network. The simulations are intended to give insights on trends and relative comparisons rather than produce accurate absolute performance metrics.

1.1.2 Next steps

More work is needed to reach the goal of effectively and efficiently supporting UEs at low altitudes while protecting and maintaining performance of ground UEs. This is true for the short term with optimizations of existing networks as well as for next generation networks that will employ new advanced technologies. Long term, our goal is to introduce techniques into next generation cellular standards that will provide simultaneous services to ground and airborne UEs optimized to meet the performance requirement of each class of device.

2 Field Trials

This chapter presents results computed from data collected at our UAS Flight Center in San Diego, California.

Flights were restricted to a cylindrical volume with 1.0 nautical mile radius and 400 ft altitude above ground level (AGL), as represented in Figure 2-1. This cylinder is centered at latitude 32.904258, longitude -117.204767.

All flights were performed in accordance with provisions in our certificate of authorization issued by the FAA.

Figure 2-1 Flight test volume

2.1 Measurement platform and data processing

Flights and measurements for this phase of data collection were performed by a custom-designed quadrotor drone, the 390QC shown in Figure 2-2.

The 390QC has a takeoff weight of 1050 grams and flight time of 16 minutes. It is equipped with the Qualcomm® Snapdragon Flight™ platform running Qualcomm® Snapdragon Navigator™ flight control software.

The drone executes fully autonomous data collection missions and can be monitored and controlled over Wi-Fi and/or LTE while in flight. An RC transmitter/receiver is active during all flights enabling immediate takeover from a ground operator for safety.

Figure 2-2 390QC quadrotor drone

The Snapdragon Flight platform connects to the LTE module capable of connecting in 700 MHz, AWS, and PCS bands.

Rich LTE modem logs are collected simultaneously with Snapdragon Navigator logs enabling correlation of flight status and data with modem logs from synchronized timestamps. Logs are stored on an SD card on the drone, and transferred (either over network or by physically moving the SD card) to a database for long-term storage.

An analysis workstation is used to manipulate database records and to produce results in the form of statistics, plots, and maps as needed. This data pipeline is illustrated in Figure 2-3.

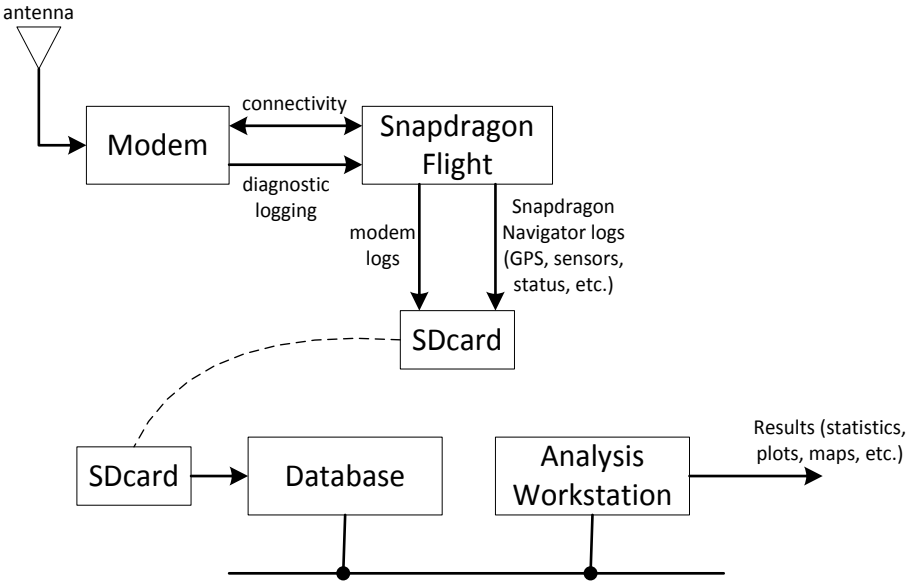

Figure 2-3 Data pipeline

2.2 Summary of data sets

For this trial, data was collected as indicated in Table 2-1.

Table 2-1 Summary of data sets

Data	Description
Location	UAS Flight Center, San Diego, California
Environment	Mixed suburban
Altitudes	Ground, 30, 60, 90, 120 meters
Test types	Mobility route at 5 m/s with 0.5 Mbps UDP UL throughput requested Mobility route at 5 m/s and periodic RACH every 15 seconds Stop/Start route with 0.5 Mbps UDP UL throughput requested
LTE bands (locked to one band per flight)	▪ PCS ▪ AWS ▪ 700 MHz
Data collection	▪ On device logging (modem and Snapdragon Navigator logs). ▪ IPerf logs

Connectivity was provided and tested using a commercial cellular network during all flights.

For analysis of UL performance and interference, we employ a method of estimating the received energy as described in Section 2.4.2 and Appendix D.

2.2.1 Mobility route

Much of the analysis in later sections is derived from a 2.5 km loop as illustrated in Figure 2-4. The figure shows flights at different altitudes, and each altitude was flown multiple times for data collection in each band, and to provide sufficient data for each case (at least two loops).

Table 2-2 lists the band and altitude permutations and the total duration for each case.

The ground data was collected by mounting the drone to a car and driving the route on surface streets (the duration of these tests tended to be a bit longer than flying due to some stoplights and traffic).

While Figure 2-4 shows flight traces including takeoff and landing from our rooftop helipad, each data set was trimmed so the final data for analysis only includes samples where the drone is at its intended altitude and underway. This prevents takeoff and landing transition data, as well as data when the drone is stationary on the landing pad, from impacting the analysis results.

NOTE: The 30 meter and 60 meter flights are slightly different from the 90 meter and 120 meter flights. The lower altitudes caused the drone to be obstructed by a high-rise building so we decided to fly in front of the building to maintain primary pilot line-of-sight visibility during those tests.

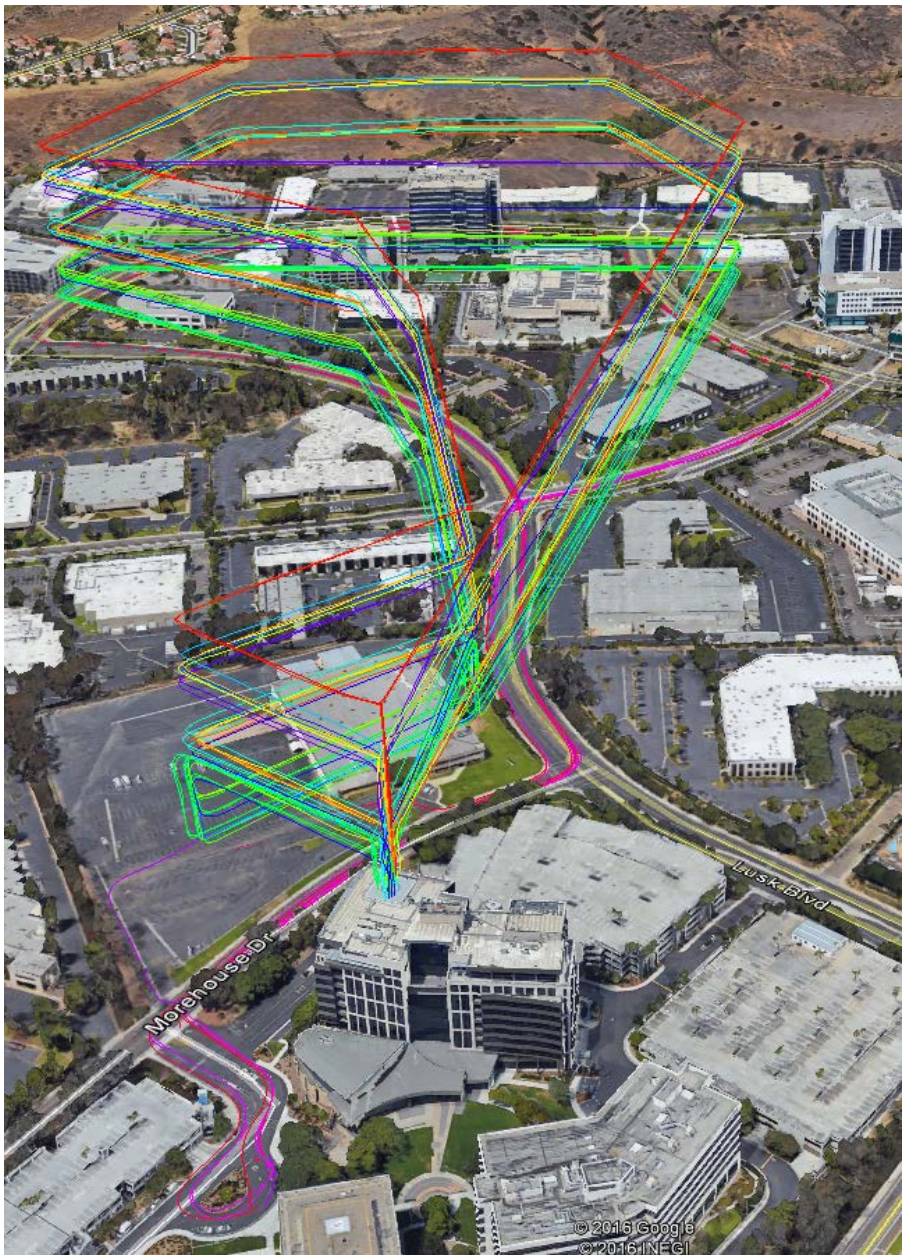

Figure 2-4 Mobility route data included in analysis

Table 2-2 Band, altitude, and duration

Band	Alt (m)	Total Time (min:sec)
PCS	0	21:36
PCS	30	12:36
PCS	60	12:33
PCS	90	32:21
PCS	120	33:12
AWS	0	27:44
AWS	30	12:31
AWS	60	12:34
AWS	90	22:52
AWS	120	15:49
700 MHz	0	34:50
700 MHz	30	18:44
700 MHz	60	12:36
700 MHz	90	16:50
700 MHz	120	15:47

2.3 Downlink: Mobility route results

2.3.1 Detected cells

We will start by looking at the number of detected cells at different altitudes and for different bands and then look at the distances to the detected cells. These views of the data do not consider received power from the cells (this comes later), just detectability.

Figure 2-5 shows a histogram of the number of simultaneously detected cells for each band and altitude. The modem at each sample point (at approximately 160 ms intervals) returns a set of detected cells with one labeled as the serving cell – this is what is meant by simultaneously detected.

The overall trend is the number of detected cells increases with altitude as expected due to the longer propagation distance of signals in the free space environments as altitude goes up. However, the trend is not without exceptions. For example, the mean number of detected cells for the 700 MHz band at 30 m is slightly lower than at the ground.

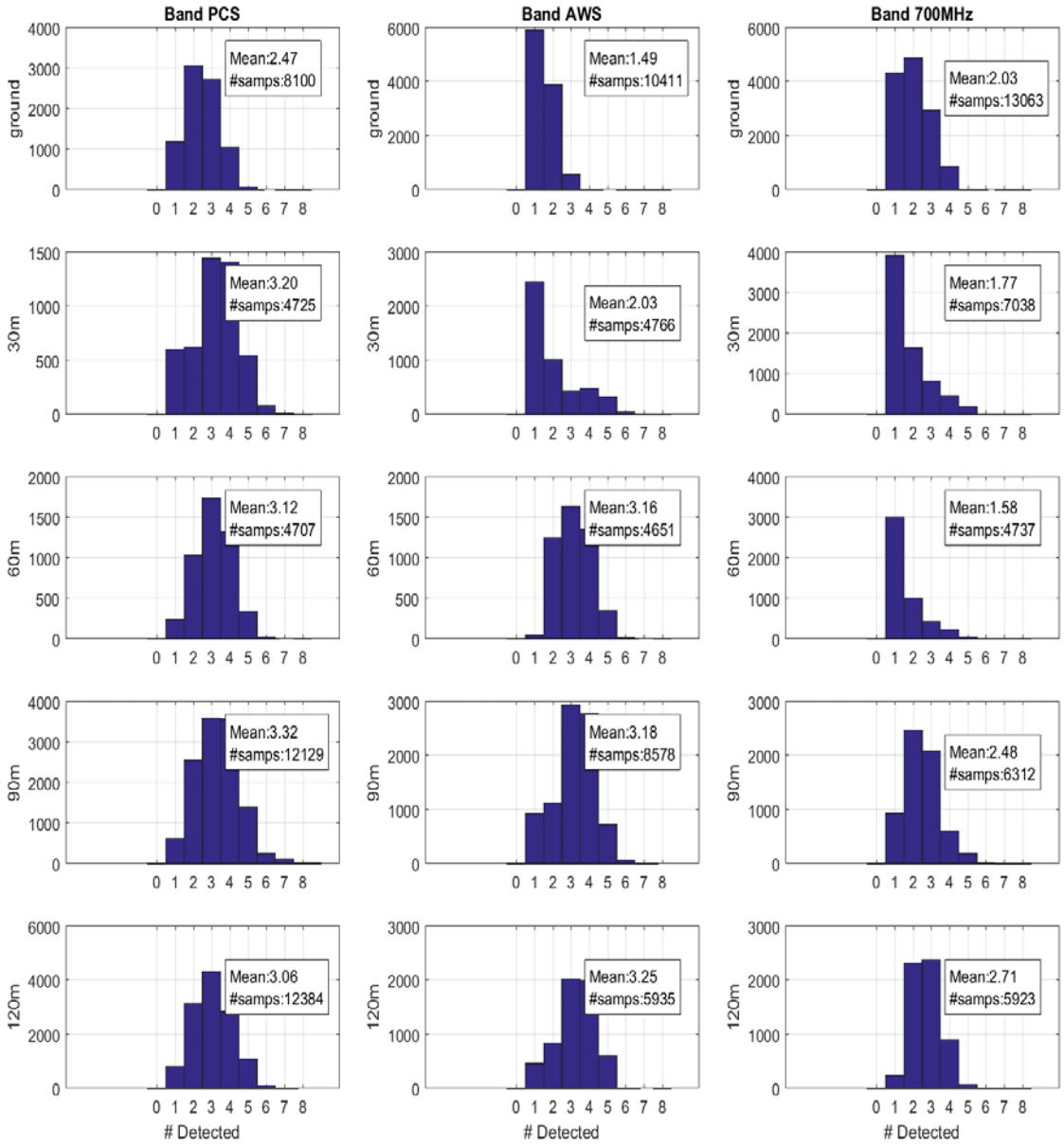

Figure 2-5 Histogram of simultaneously detected cell reference signals

An alternate view of cell detectability is the distance distributions to detected cells. Here we consider all detections independently rather than grouping them by their detection instant. Figure 2-6 displays these distributions for each band. The top row of figures shows the serving cells only, and the bottom row considers all detected cells (including serving).

Focusing first on the ground curves (in blue), all serving cells are within 1 km and virtually all neighbors within 2 km for all 3 bands. However, this changes significantly as we look at the nonground curves. Serving cell distance distributions for Bands AWS and 700 MHz are only mildly impacted by altitude, however PCS sees a more significant change. For example, >15% of PCS serving cells are at distance of > 5 km at 60 m altitude.

Looking at all cells, altitude has a clear impact on the probability of detecting distant cells. It is surprising to see the impact appear much more severe for PCS than 700 MHz. AWS is in the

middle. The difference could be explained by the different numbers of cells in each band deployed in the test area.

It is also counterintuitive that the data shows such longer distances to detectable PCS cells than 700 MHz given that 700 MHz is expected to propagate further than PCS at 1900 MHz. PCS and 700 MHz antennas are different with different pointing and different gain patterns, which are likely contributors to the observation of different detection distances.

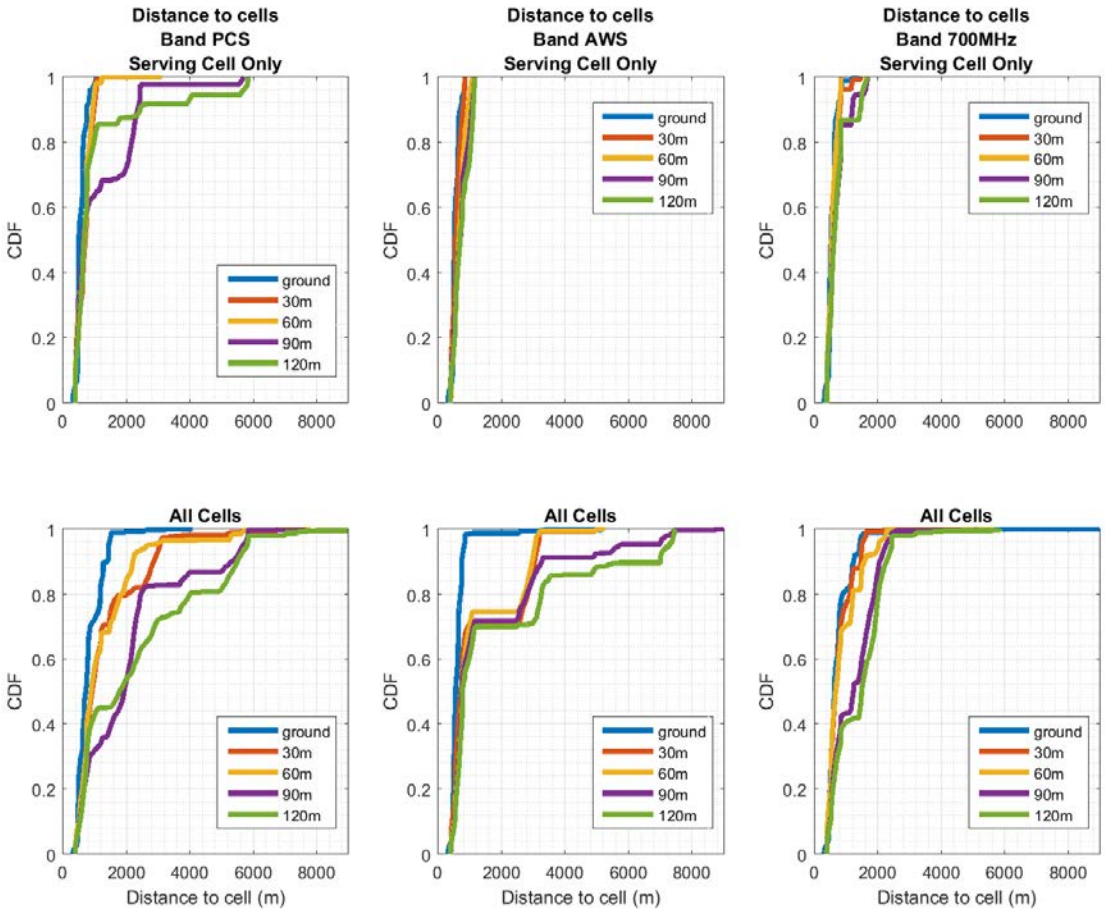

Figure 2-6 Distribution of distance to detected cells; top row includes only serving cells, bottom row adds all neighbor cells

2.3.2 Serving cell analysis

Now we take a closer look at serving cell data. The serving cell physical cell indicator (PCI), reference signal received power (RSRP) and reference signal received quality (RSRQ) are collected during test flights for each band and altitude combination. Depending on the band and altitude, we see as many as six serving cells and as few as one in a flight over the mobility route.

In Figure 2-7, a representative flight was chosen for each band and altitude combination and the RSRPs are displayed. (While other flights do not show identical results, they are similar qualitatively to these). The RSRPs shown on the maps can be viewed using the color bars for each plot, where higher strength signals with larger RSRP are lighter in color, and lower strength signals are darker.

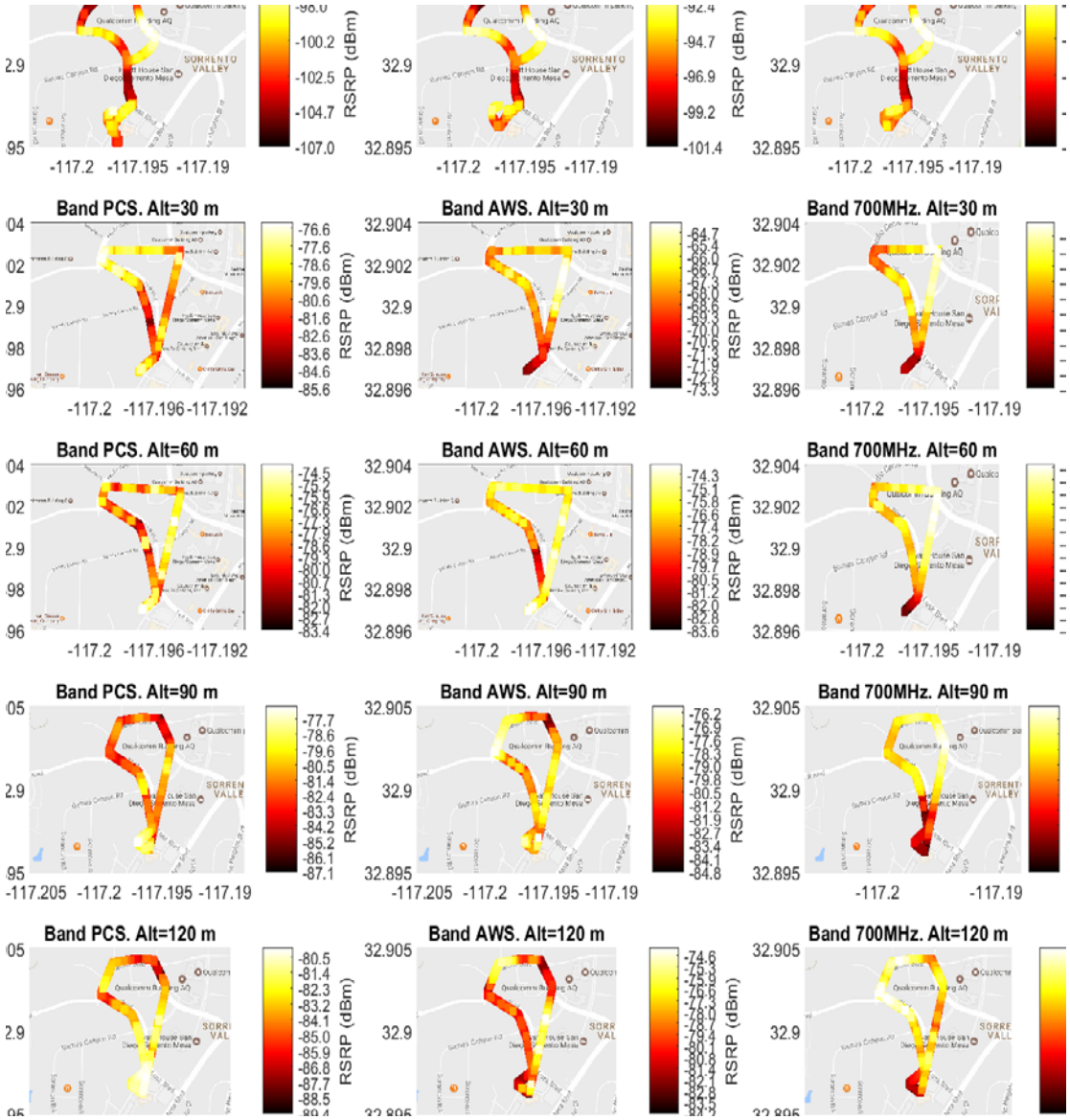

Figure 2-7 Maps of selected sample flights showing serving cell RSRP; the color bar scale is different for each map

The distributions of the serving cell RSRP and RSRQ are shown in Figure 2-8 which allows a direct comparison across altitude and band. Ground RSRPs are lower than at altitude in general, though the high tail of the ground RSRP distribution shows the highest RSRPs of all. This is expected to be due to the higher chance of a ground user experiencing a direct line-of-sight directly into the main beam of the cell antenna. The fact that airborne users see stronger serving cell RSRPs than ground users has been surprising to some who expect the downtilted antennas to weaken signals significantly to airborne users. These results indicate that the stronger free space propagation to airborne users does in fact make up for antenna gain reductions.

The RSRQ distributions however give an indication that interference grows with altitude until 400 ft above ground. Median RSRQ reductions of 10 dB for the highest altitudes relative to ground are seen for Bands PCS and AWS and reductions of 4 dB for 700 MHz. The better relative RSRQ performance of 700 MHz may be due to the antenna downtilt and gain pattern difference across bands.

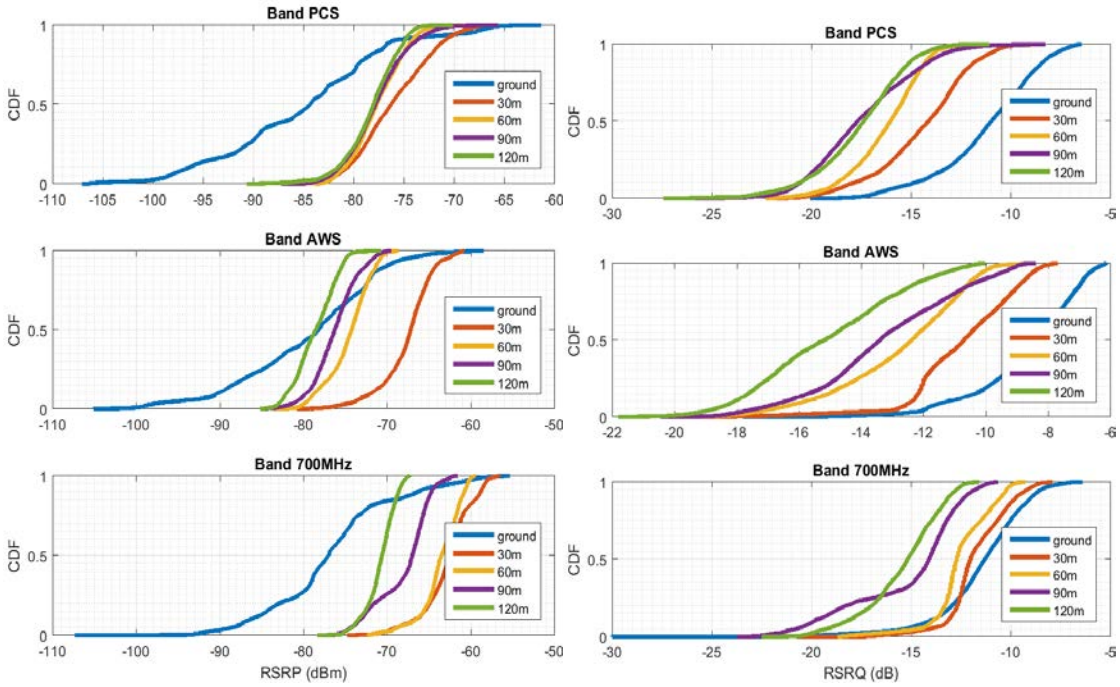

Figure 2-8 Distributions of serving cell RSRP and RSRQ for each band and each altitude

One way to visualize and analyze the simultaneous dependence of RSRP and RSRQ with altitude changes is using the scatter plots in Figure 2-9. Here, each point is a single sample with RSRP (dBm) on the x-axis, RSRQ (dB) on the y-axis, and colored with the altitude associated with the sample. Lighter colors represent higher altitude (see the color bar legends).

In this visualization, the dependence becomes even clearer. Ground level samples cover a large range of RSRP and RSRQ. As altitude goes up, the range of values becomes tighter with generally stronger RSRP but depressed RSRQ. This behavior is similar for all three bands.

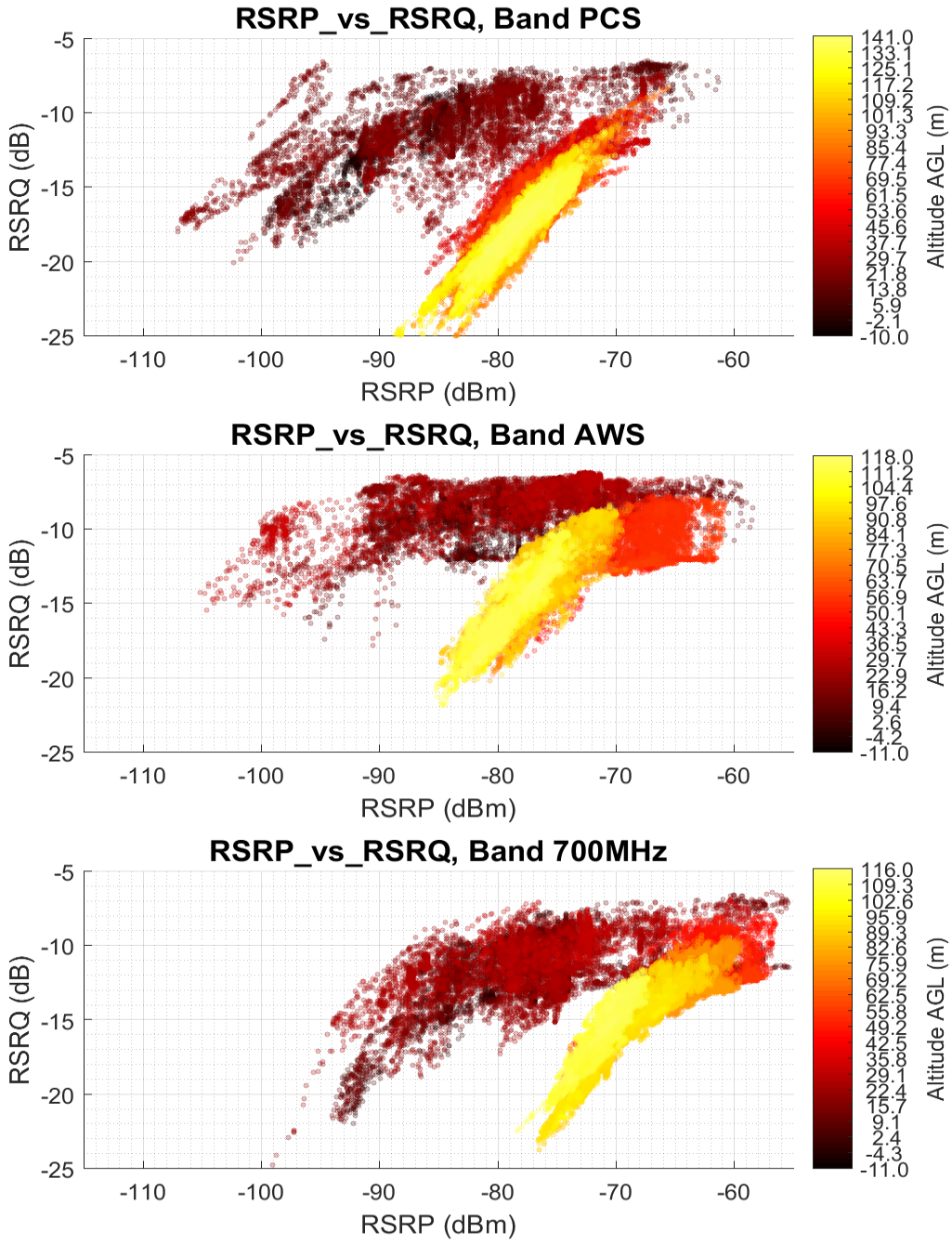

Figure 2-9 Scatterplots of serving cell RSRP vs. RSRQ for each band; points are colored by altitude (see color bar scale)

2.3.3 Neighbor cell analysis

In this section, we expand to the analysis of neighbor cell detected signal characteristics. Because the relative strength between detected cells is an important factor for both handover algorithm performance and interference impact, we look at differences between detected signal RSRPs in dB.

Figure 2-10 shows the distributions of the difference (Delta) between the serving cell RSRP and the *n*th strongest neighbor RSRP detected at the same instant.

The first row of plots shows the first strongest neighbor, the second row shows the second strongest, third row the third strongest, and fourth row the fourth strongest neighbors. There is data for more neighbors, but it becomes less significant so we truncate the plots to the fourth strongest.

Data for each band is shown in a separate plot as before. Thus, a point on the distribution represents the probability that at least the required number of neighbors is seen and the Delta RSRP is less than or equal to the value on the x-axis. The curves can be seen to plateau before reaching a probability of 1.0 due to the probability the nth neighbor is not detected at all.

Note that negative Delta RSRP (RSRP inversion) values occur only when the serving cell is not the strongest cell. While this is not desirable in general, it often results even when the handover algorithm is fully optimized due to hysteresis parameters used to prevent rapid, or ping-pong handoff occurrence in the presence of highly dynamic signals particularly during mobility.

Focusing first on the first strongest neighbor distributions, several points can be noted:

- For all bands, the probability of RSRP inversion for ground tests is less than 10%, but as the altitude increases, this probability goes up.
- Because handover trigger threshold is typically set to a small negative Delta RSRP (or RSRQ depending on the network configuration), higher probabilities of Delta RSRP in this range (say -3 dB to 0 dB) indicate a larger likelihood of interference and cell edge conditions during flights in the network at altitude than on the ground.

For the second strongest neighbors, the ground data shows a negligible amount of energy for Bands AWS and 700 MHz and a small amount for PCS. However, as altitude increases, the contribution of the second strongest cell to interference becomes non-negligible. Similar conclusions are displayed for the third and fourth strongest.

In studying this data, it is also clear that precise regularity in the results is not achieved, such as strictly monotonically increasing interference with altitude. For example, the distribution of second strongest interference for 700 MHz is noticeably higher at 90 m than for 120 m. We expect these kinds of results occur due to flights occurring in a limited geographical space in the network.

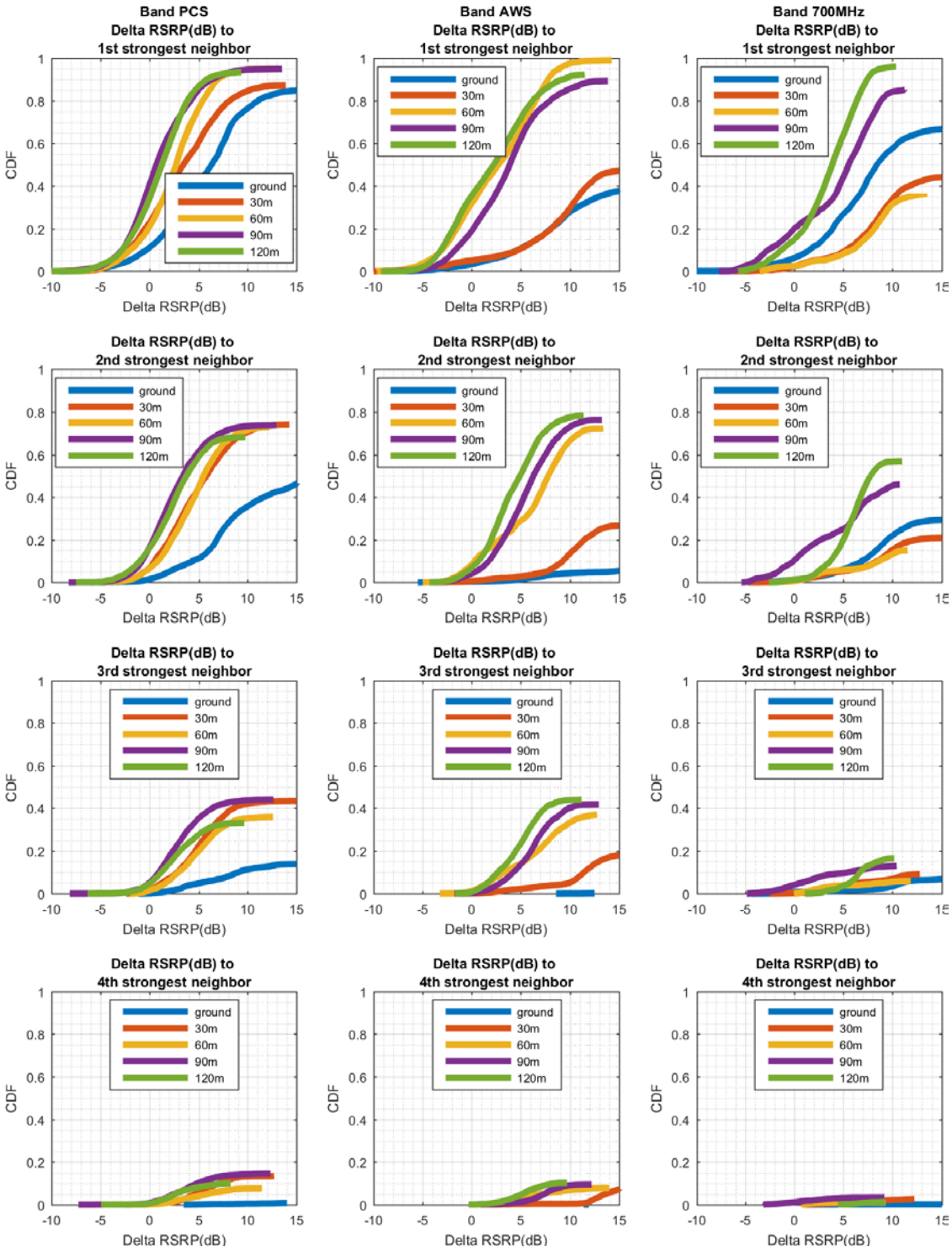

Figure 2-10 Distributions of DeltaRSRP ($RSRP_{serving}$-$RSRP_{neighbor,i}$)

The results discussed rely on serving cell selection since the data are relative to serving cell RSRP, thus are impacted by the handover algorithm and its operational parameters.

Figure 2-11 shows distributions of the same data, but using a slightly different metric we call Delta RSRPall. This metric computes the relative RSRP to the strongest cell always, and thus is independent of the serving cell selection (handover) algorithm. These distributions can be used to understand results based only on network layout and signal propagation. Note the Delta RSRPall metric is >0 by definition. We will not discuss these plots in detail here, and leave interpretation to the reader.

Finally, the scatter plots in Figure 2-9 for serving cell measurements can be augmented to include all measurements (serving plus neighbor cells). This is shown in Figure 2-12. As can be seen, the overall character of the data is similar, but with many more sample points. The reported RSRQ has a lower limit of -22 dB, which is visible in the plots.

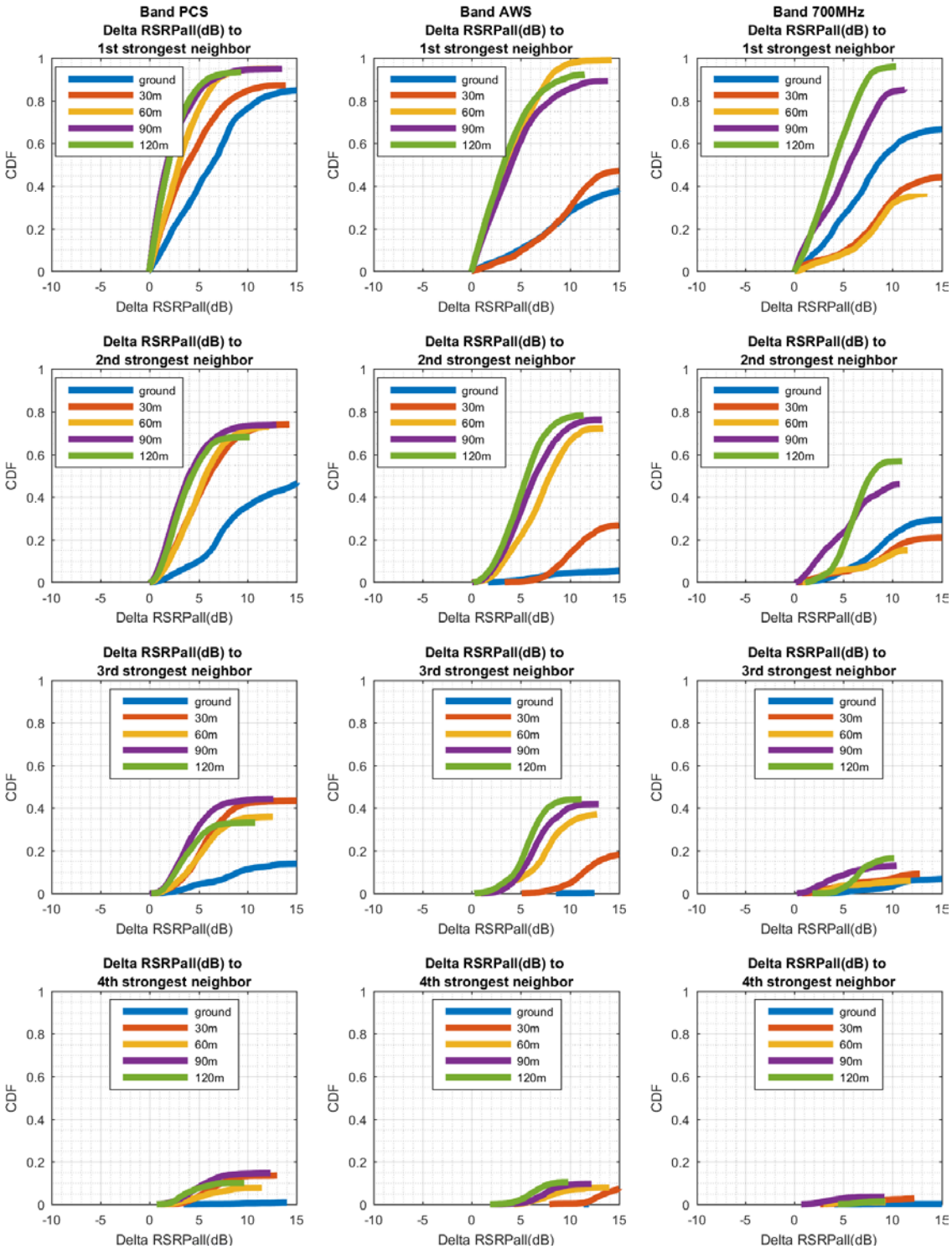

Figure 2-11 Distributions of Delta RSRPall

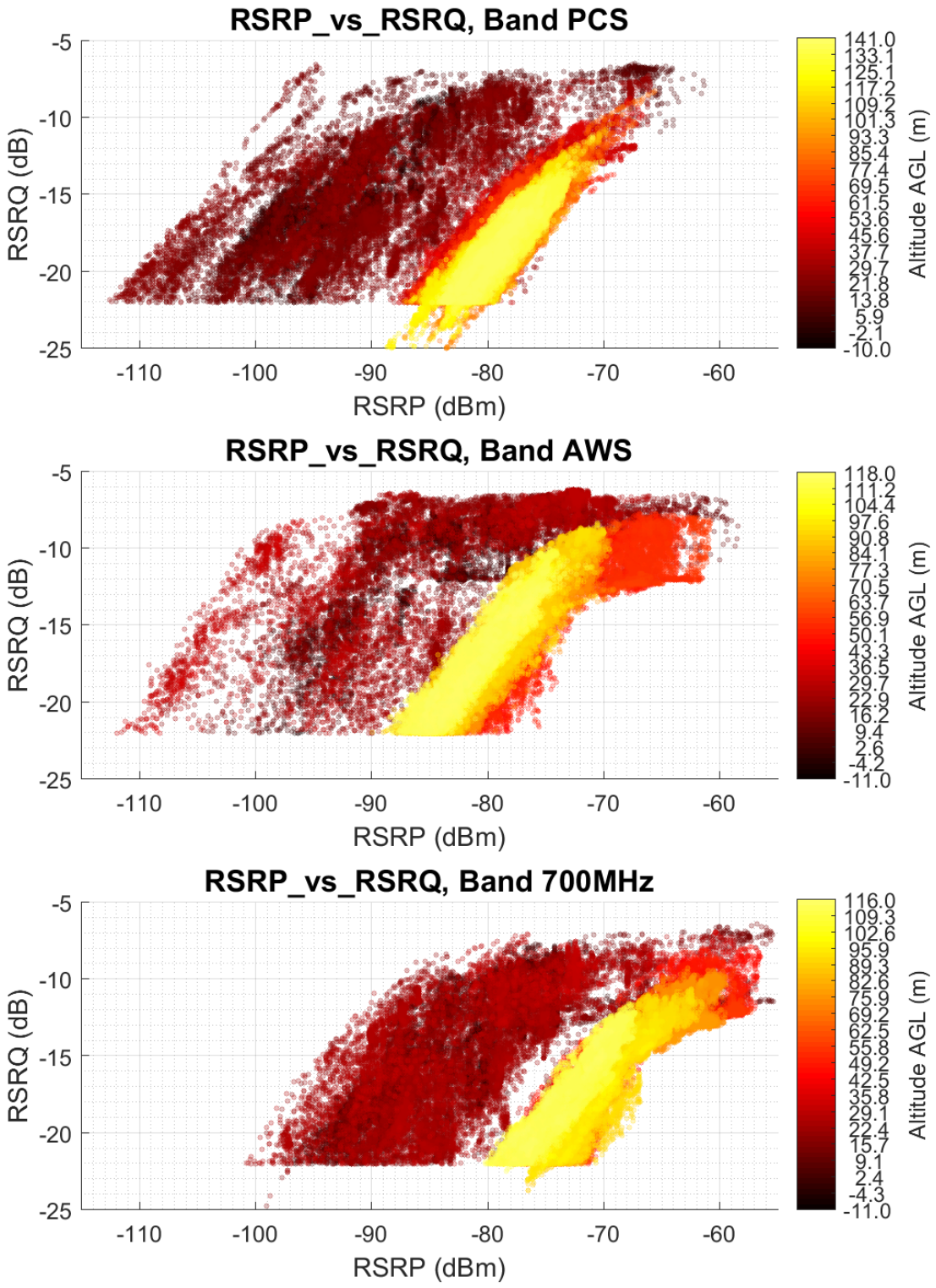

Figure 2-12 Scatterplots of RSRP vs. RSRQ for all detected cells for each band; points are colored by altitude (see color bar scale)

2.4 Uplink power and interference results

2.4.1 Transmit power

In this section, we discuss uplink results obtained from flights with a constant UL data stream of 0.5 Mbps sent from the drone to our trial ground server.

This is a relatively low data rate consistent with what would be required for a medium quality video stream. While future applications may demand higher rates, our intent here was to produce data enabling comparisons of performance across different altitudes without placing an undue burden on the commercial network during our trial flights. Tests of the limits of UL (and DL) throughput in flight are a suggested topic for future study.

Total transmit power and the number of resource blocks (RBs) assigned as a function of time were logged during flights. This transmit power is determined by power control (Refer to Appendix C, *3GPP Technical Specification 36.213*.)

$$P_{TX} = \min(P_{max}, 10log_{10}(M) + P_0 + \alpha \cdot TPL + f) \quad (2\text{-}1)$$

where

P_{max} = maximum power

M = number of RBs assigned

P_0 = nominal value

α = path loss scaling

TPL= estimated total (including antenna gains) path loss

f = accumulated closed-loop transmit power control (TPC) commands

Figure 2-13 presents the distribution of transmit power per resource block (RB), 200 kHz per RB in the 700 MHz band. The larger path loss experienced on the ground causes larger transmit powers. Then the trend observed is that the transmit powers drop when in flight with narrowed distribution, but grow as the altitude of flight increases until about 400 ft above ground.

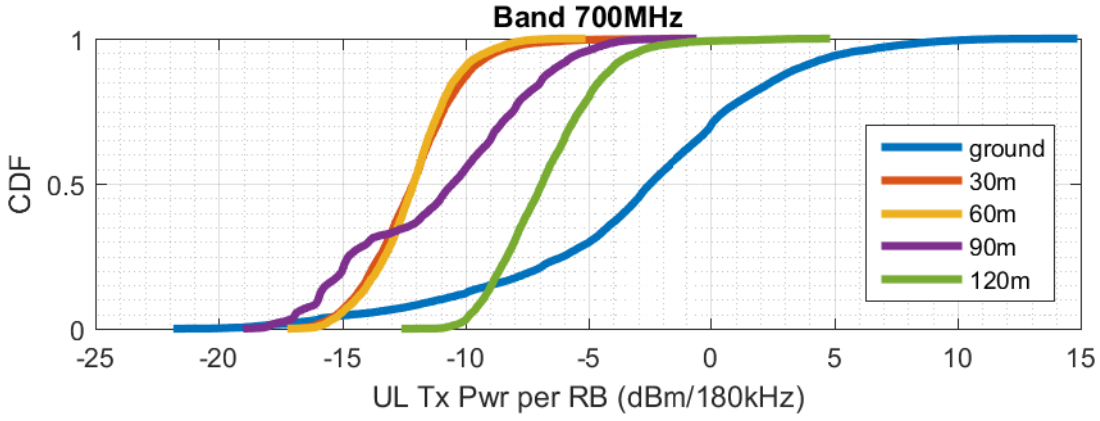

Figure 2-13 Distribution of uplink transmit power density (per RB)

2.4.2 Estimated uplink interference

While the transmit powers in flight are lower, we expect from the DL RSRP results that since differences between total path loss (TPL) of serving and neighbor cells are smaller in flight than on the ground, these transmissions arrive at the neighbor cells with relatively high power.

Measuring these received powers at the cell is desirable, but due to the difficulty of attributing received energy to a single device in logging (at time of publication), this measurement was not available. However, it is possible to predict the received energy at a cell by assuming channel reciprocity between the DL and UL, and thus use the DL TPL estimate as an estimate of the UL TPL as well. This path loss can be estimated as

$$TPL_{est} = P_{TX,cell} - 10log_{10}(12 \cdot BW) - RSRP \quad (2\text{-}2)$$

where

$P_{TX,cell}$ = total DL maximum transmit power for the cell

BW = transmission bandwidth for the cell in RBs (eg. 50 for 10 MHz)

$RSRP$ = the measured RSRP at the device from this cell

The second term simply scales down the total transmit power to the portion allocated to the reference signal.

This method of estimating UL received energy is described further, including lab test validation, in Appendix D.

Using this estimation of cell received power, we now look at distributions of power seen at neighbor cells. While the received power at the serving cell is carefully controlled for successful UL demodulation, the power at the neighbors is interference that impacts the overall uplink capacity of the network. Figure 2-14 shows distributions of received energy per RB across all neighbor cells detected in the trial data for 700MHz.

The gap in these distributions across altitudes gives a statistical notion of the increase in interference produced. The gaps at the median are approximately 5 dB for 700MHz. This means a device at altitude can contribute 3 times the interference in the network in 700MHz than a ground user.

Figure 2-15 shows a slightly altered view of this data. Here, the transmit powers per RB are scaled up to the power that would be seen if the drone had been utilizing all RBs in the system, but capping the maximum transmit power at 23 dBm. The distributions are similar, but clearly scaled up to full power. Also, the transmit power cap is seen to only influence the ground curve as this is much more likely to be impacted by transmit power cap.

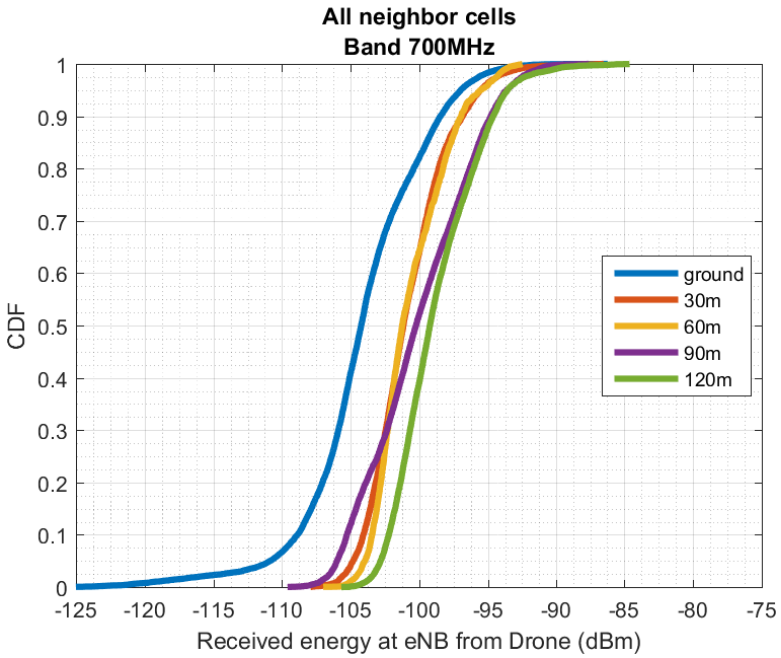

Figure 2-14 Distributions of estimated uplink interference density at neighbor cells due to drone transmissions; interference is estimated assuming path loss measured on downlink is equivalent to uplink path loss for each cell

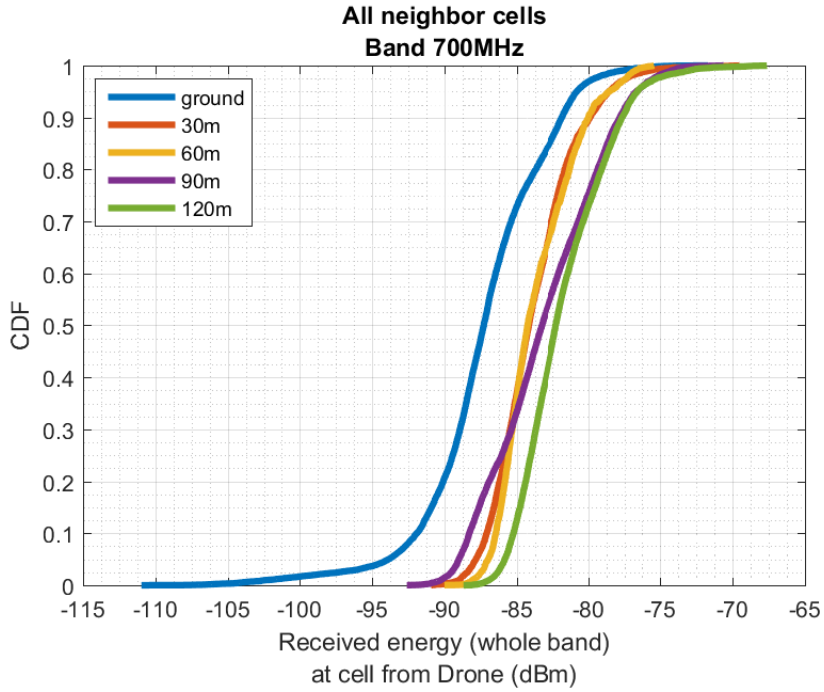

Figure 2-15 Distributions of estimated total uplink interference at neighbor cells due to drone transmissions; here transmit power from drone is scaled up to the whole band (all RBs) subject to 23 dBm maximum transmit power

2.5 Handover analysis

Handovers occurred during trial data collection a total of 206 times.

Figure 2-16 shows distributions of the total interruption time during handovers. The majority of these are between 20-40 ms, but there are some outliers present as high as 800 ms. While these are not large interruption times, it is notable that the outliers are more likely in this data at altitudes 60 meters and higher.

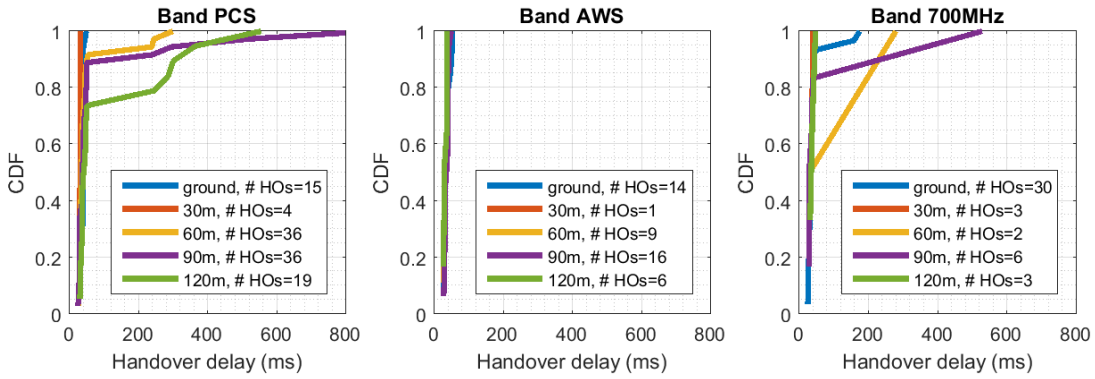

Figure 2-16 Handover events and distributions of delay in handover completion

2.6 Path loss modeling

Since it is expected that propagation differences at altitude relative to ground is one of the principal contributors to the different performance of the network for drones, we will look at path loss results from the field data.

Here, path loss is considered to be only the over-the-air contribution without the effect of cell and drone antenna gain patterns. TPL or total path loss is the term used here when antenna effects are included, such as in Section 2.4. We use RS transmit power minus RSRP as the TPL (including antenna effects). Thus to study the over-the-air portion, it is necessary to estimate the antenna gain at both the transmitter and receiver and eliminate these from the total path loss measured.

$$PL_{est} = P_{TX,cell} - 10log_{10}(12 \cdot BW) - RSRP + G_{drone} + G_{cell} \quad (2\text{-}3)$$

where

$P_{TX,cell}$ = total DL maximum transmit power for the cell

BW = transmission bandwidth for the cell in RBs (eg. 50 for 10 MHz)

$RSRP$ = the measured RSRP at the device from this cell

G_{drone} = antenna gain at the drone

G_{cell} = antenna gain at the cell

Antenna gains are obtained assuming a line-of-sight path from the cell antenna to the drone. This requires the relative positions of the cell and the drone to be known at all times, and the orientation (or attitude) of both the drone and the cell antennas are known in the global frame. Drone position and orientation (pitch, roll, and heading) are measured from the onboard flight controller, and cell antenna location and orientation (azimuth and downtilt) are known from a cell site database.

The drone antenna pattern for each band was measured in an antenna chamber using the fully integrated drone package. These results are shown in Appendix E.1.

The base station cell antenna gain patterns are obtained from manufacturer published patterns. We used unique patterns for each antenna type, frequency band, and electrical downtilt value. An example base station antenna pattern is shown in Appendix E.2.

Results obtained using this technique are by nature approximate. We are using cell antenna patterns obtained during manufacturer testing in controlled environments, while the field measurements are obtained using antennas mounted in many different configurations and on different types of structures. The installed antenna patterns will be impacted by each particular installation. Further, direct line-of-sight is used for looking up the antenna gains, however reflected signals can have an important contribution to total power detected, especially for ground tests. Nevertheless, the analysis making these significant approximations is presented here as it still gives insight into the differences between propagation at different altitudes.

Figure 2-17 shows these path loss samples as a function of distance from the drone to cell. Bands PCS, AWS, and 700MHz are plotted separately. The top row of plots shows serving cell samples only, and the bottom row adds neighbor cell samples. In addition to the sample point, analytical path loss models with exponent 2.0 and 4.0 are shown for reference given that those slopes are commonly used for free space and ground models respectively.

One use of this type of analysis is guiding the path loss models for simulations. These results indicate the free space model (exponent 2.0) is a viable model to use for airborne vehicles in simulations. Here the free space model is

$$PL = 20log_{10}d + 20log_{10}\frac{4\pi f}{c} \quad (2\text{-}4)$$

with d being distance in meters, f frequency in Hz, and c speed of light in m/s.

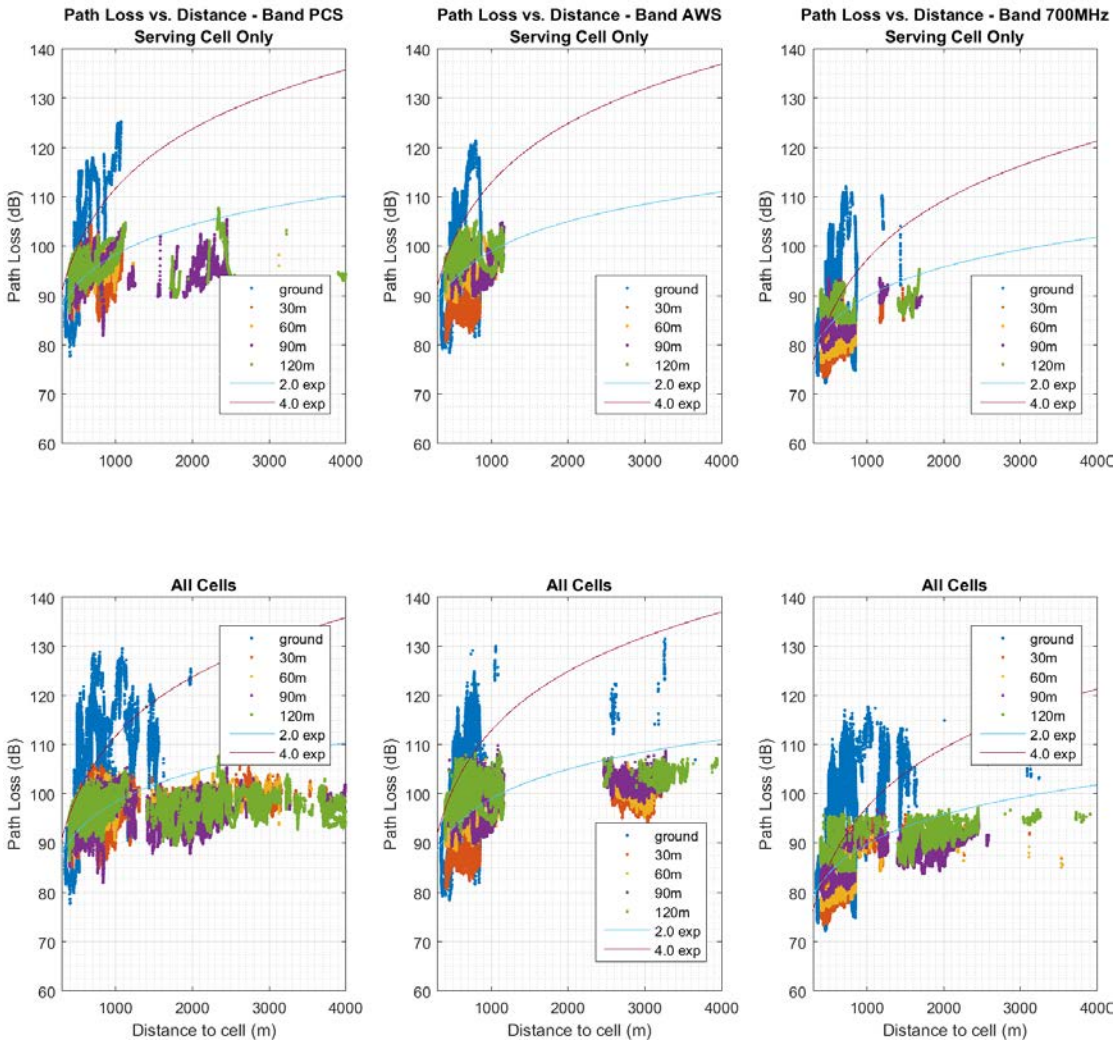

Figure 2-17 Path loss as a function of distance; top row is serving cell measurements only, bottom row adds neighbors

3 Simulations

3.1 Goals and scope

The simulations performed for this trial were designed to study of performance tradeoffs when the network is serving many ground and airborne UEs simultaneously over a wide area. The simulations follow 3GPP system simulations guidelines for network layout and ground channel modeling.

Here we present studies of:

- Downlink SINR
- Uplink interference and throughput
- Mobility performance with airborne UEs in the network

The goal is to give insights into the techniques that can be expected to provide the best payoff for overall performance of both ground and airborne UEs as the number of airborne UEs grows in the future. This also guides the plans and design of next-phase field trials to make sure such trials focus data collection and analysis on the most promising techniques. Note the simulation results are dependent on the evaluation methodologies including the network layout, propagation model and product implementations, and therefore should not be treated as the accurate absolute performance of actual networks.

3.2 Setup and assumptions

The simulations performed used the setup described in Table 3-1.

Table 3-1 Simulation setup

Item	Description
Layout	▪ The layout follows the 3GPP D3 layout for system simulations in *3GPP Technical Specification 36.814 v9.0.0* (see Appendix C) with antennas modified for this simulation. ▪ The D3 layout is a hexagonal grid with 1732 meter site-to-site spacing, and 3 cells per site (pointed in 120 degrees azimuth increments). ▪ Due to the importance of the 3D antenna pattern for these simulations, the standard 3GPP simulation antenna was replaced with a 3D model of a representative commercial antenna, the 80010734_716MHz antenna (shown in Appendix E.2). ▪ Six degree mechanical downtilt was used for all antennas, and the total transmit power limit was set to 46 dBm.
Band	▪ 700 MHz band only, with 10 MHz bandwidth

Item	Description
Propagation modeling	▪ Ground UEs are modeled using the 3GPP typical urban profile number 3 (TU3), refer to Appendix C, *3GPP Technical Specification 36.814 v9.0.0*. This model uses a path loss exponent of 3.76 and log-normal shadowing with standard deviation 8.0 dB. ▪ Drone UEs are all modeled with free space propagation and zero shadowing. This model uses a path loss exponent of 2.0. The explicit formula (in dB form) is provided in Section 2.6.

3.3 Downlink simulations

Downlink results are captured by the SINR distribution computed in the simulation assuming full-buffer traffic.

The simulator randomly and uniformly positions UEs in the network and then computes the received signal energy at each UE from all of the cells using the relevant propagation model and the cell parameters such as antenna gains and transmit power.

Multiple samples are produced to randomize the UE locations in space and random model parameters such as log-normal shadowing. Then SINR is for a particular UE is

$$SINR = \frac{S_i}{N + \sum_{\substack{j=1 \\ j \neq i}}^{M_c} S_j} \qquad (3\text{-}1)$$

where S_j is the signal power received from the *j*th cell. *i* is the index of the strongest signal (serving cell) and M_c is the number of cells. Thus, the *SINR* is the serving cell signal power divided by the sum of all other signal powers plus thermal noise, *N*.

The received signal power is computed starting with the transmit power at the cell, applying the antenna gain (or attenuation) in the direction of the UE, and then applying the propagation losses from the propagation model relevant to that UE. For UEs at altitude, it is much more likely the strongest signal will come from outside the main beam of a cell than for UEs on the ground. This is the reason we used a commercial 3D antenna pattern that accurately models the gain in all directions for these simulations.

This distribution gives a statistical picture of the signal quality that can be expected by users in the network. Since this distribution for users at one altitude is not affected by users at other altitudes, we perform these assumptions with all users at a single altitude, one altitude at a time.

3.3.1 Analysis of results

Downlink SINR distributions from simulations of users at ground level, at 50 meters altitude, and at 120 meters altitude are shown in Figure 3-1.

First we observe that the distribution for 50 meters and 120 meters are essentially identical. This indicates that, for this layout, the distribution is dominated by the propagation model differences between the ground and airborne UEs. We note a few key observations from these distributions:

- SINRs are lower for airborne UEs, and this is expected due to the higher levels of interference from neighboring cells experienced due to the free space propagation of signals. The median degradation relative to ground users is approximately 5 dB.
- The outage probability (defined here as SINR < -6 dB) from these simulation results is very similar for ground and airborne users, and is approximately 1%. DL spectral efficiency of

140 kbps/MHz can be expected at -6 dB, and this would allow for 1.4 Mbps throughput given a 10 MHz allocation.

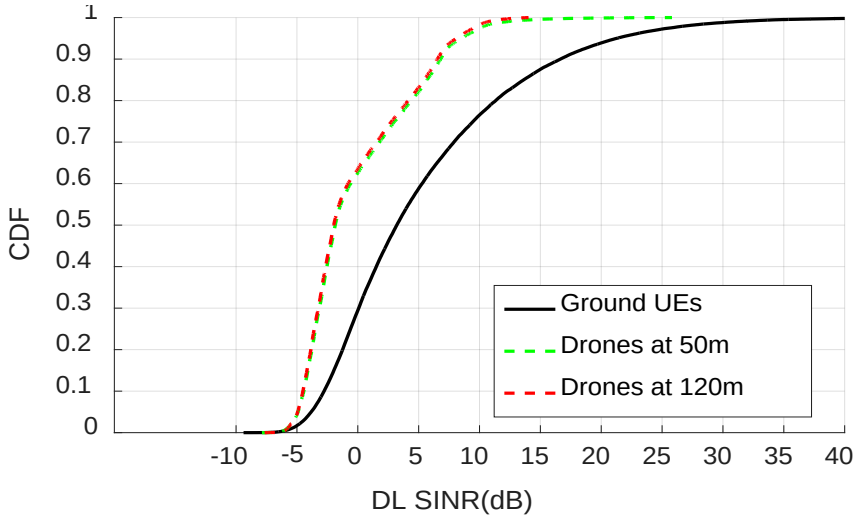

Figure 3-1 Distributions of downlink SINR for UEs at ground, 50 meter, and 120 meter altitudes

3.4 Uplink simulations

Uplink simulations are performed to study the impact of altitude on interference levels at the cells and throughputs available to UEs.

In contrast to full-buffer downlink simulations, uplink performance for a UE depends on the specific location (including altitude) and transmissions from neighboring UEs because they directly interfere with one another. Thus it no longer makes sense to simulate all UEs at a single altitude as we did for the downlink simulations. Here we fix the number of UEs per cell to 30, and perform simulations that vary the split of these users between ground level, and altitude. Here we selected 120 meters for all drone UEs.

We focus on power control and resource partitioning as techniques for performance improvement. Some techniques require the network to distinguish between UEs at altitude and those on the ground to be effective, but other techniques can treat all UEs the same. Clearly it is simpler to use a method that does not require such UE identification, and we discuss this during the presentation of the results.

We make use of the interference to thermal (IoT) ratio metric in these studies. This metric sums the contribution of received signal energy from all UEs served by neighboring cells and divides this by thermal noise. The plot axes are labeled *preMMSEIoT* to emphasize this metric is computed prior to the processing in the receive demodulator.

Features are studied here without making reference to the precise feature design and configuration implemented in today's networks. For example, there is no claim that the power control algorithms studied here are equivalent to the implementation in the commercial network studied in the Chapter 2 field trials. However, comparative study between algorithms can still be used to gauge the relative benefits of different approaches.

3.4.1 Analysis of results – power control

Figure 3-2 shows IoT distributions resulting from simulations using a baseline open loop power control (OLPC) algorithm. This power control algorithm is written

$$P_{TX} = \min(P_{max}, 10log_{10}(M) + P_0 + \alpha \cdot TPL) \quad (3\text{-}2)$$

where

P_{max} = maximum power

M = number of RBs assigned

P_0 = nominal value

α = path loss scaling

TPL= estimated total (including antenna gains) path loss

Here, P_{max}= 23 dBm, $M = \frac{5}{3}$ RBs per UE when scheduled, P_0 = -84 dBm, and α = 0.7.

Five cases were simulated – all ground UEs, all drone UEs, and splits of 3.5%, 17%, and 50% drone UEs. Since there were approximately 30 UEs per cell for these simulations, this translates to, on average, 1, 5, and 15 drone UEs per cell.

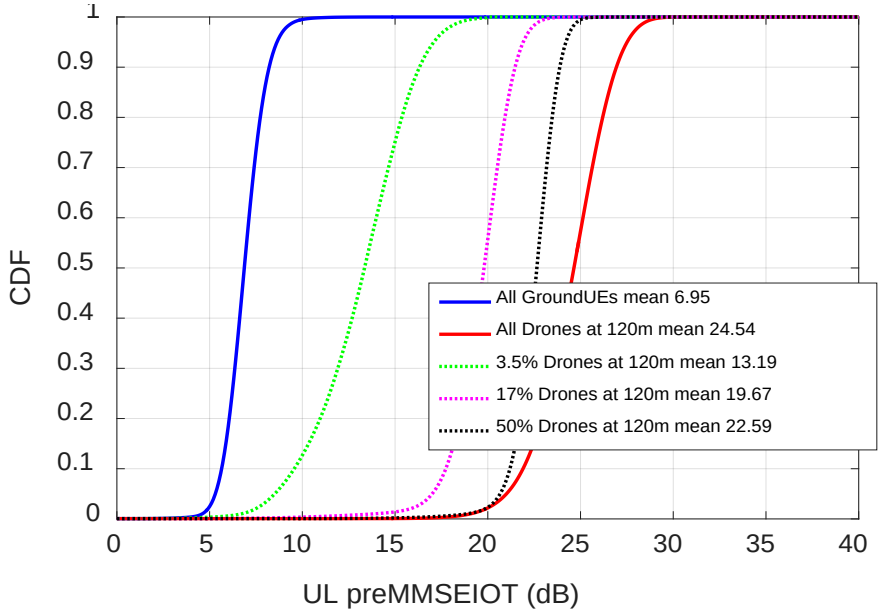

Figure 3-2 IoT distributions with baseline OLPC

As seen in Figure 3-2, the IoT for all ground users has a median of 7 dB with a distribution essentially contained between 4 dB and 10 dB. This distribution and is the result of optimizing the algorithm parameters for this case targeting a 7 dB median.

However, it is immediately apparent that the existence of drone UEs has a big impact on UL interference with these power control settings. Adding one 120 meter drone UE raises the median IoT to 13 dB. With half of the UEs being drones, the drone UEs dominate the interference produced. While these are high interference levels in the network, it should not be surprising that power control parameters optimized for ground propagation are not effective for users experiencing free space propagation.

Next we present three power control techniques that mitigate this interference issue and discuss their implementation and the IoT resulting from these techniques.

Adaptive OLPC

This is an open loop power control algorithm that is the same as before, but with different P_0 and α parameters used for UEs at altitude than for ground UEs. Thus the parameters are *adapted* to the UE type. This algorithm has the disadvantage that UEs at altitude need to be identified such that these different parameters can be used. The drone UE parameters are changed to P_0 = -98 dBm, and α = 0.7.

Optimized OLPC

This is a modified open loop power control algorithm using not only the path loss estimate to the serving cell, but also the path loss estimate to the neighbor cell most impacted by the UEs transmissions (the one with the smallest path loss among detected neighbors). This algorithm can be employed by all UEs without differentiation of airborne and ground UEs. This power control algorithm is written

$$P_{TX} = \min(P_{max}, 10log_{10}(M) + P_D) \quad (3\text{-}3)$$

$$P_D = \min(P_0 + \alpha \cdot TPL_0, P_1 + TPL_1) \quad (3\text{-}4)$$

where

P_{max} = maximum power

M = number of RBs assigned

P_0 = nominal value

α = path loss scaling

TPL_0= estimated total (including antenna gains) path loss to the serving cell

P_1 = nominal value for strongest neighbor

TPL_1= estimated total (including antenna gains) path loss to the strongest neighbor cell

Here P_0 = -84 dBm, α = 0.7 and P_1 = -98 dBm.

CLPC

This is a closed loop power control (CLPC) algorithm run by the serving cell that takes into account interference conditions in other cells.

When interference over thermal value in a given cell exceeds the threshold value, interference overload indication is transmitted over the backhaul link to all neighboring cells.

When a cell receives overload indicator bit set to high, the eNB that controls uplink power, generates closed loop power control commands to the UEs it serves, instructing the UEs to reduce transmit power. If not, eNB is free to send closed loop power control commands for power increase or no change. The power control formula used in this scenario is given by

$$P_{TX}(i) = \min(P_{max}, 10log_{10}(M) + P_0 + \alpha \cdot TPL + f(i)) \quad (3\text{-}5)$$

where

$f(i)$ = accumulated close loop power control adjustment at time i

Figure 3-3 through Figure 3-5 show the IoT distributions for each of these power control techniques.

First we note that they all provide significant improvements relative to the baseline Figure 3-2.

The Adaptive OLPC reduces median IoT for all drones from 25 dB to 12 dB, a significant change.

The Optimized OLPC method provides very good control of interference even without requiring identification of UEs at altitude. Figure 3-4 shows very similar IoT distributions from 0% to 50% drone UEs, and even moderate increase in interference for the case of 100% drones.

CLPC also provides control of interference magnitude, but, as shown in Figure 3-5, the high tail of the distribution is quite long compared to optimized OLPC.

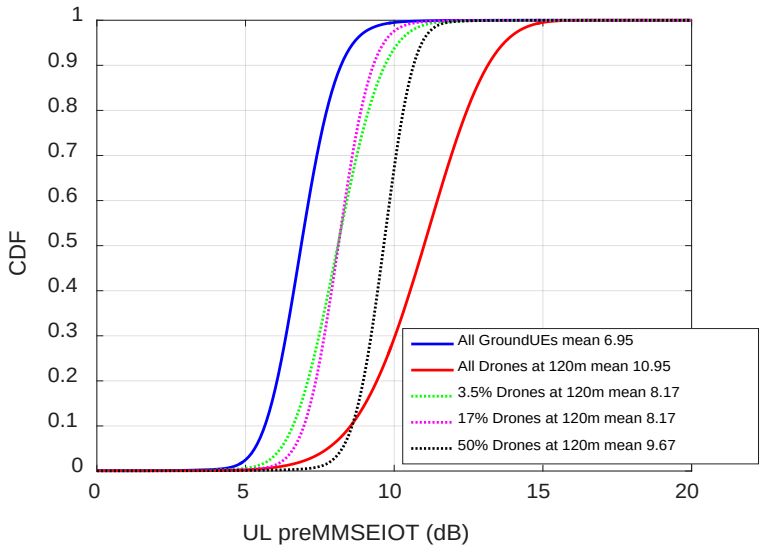

Figure 3-3 IoT distributions for Adaptive OLPC

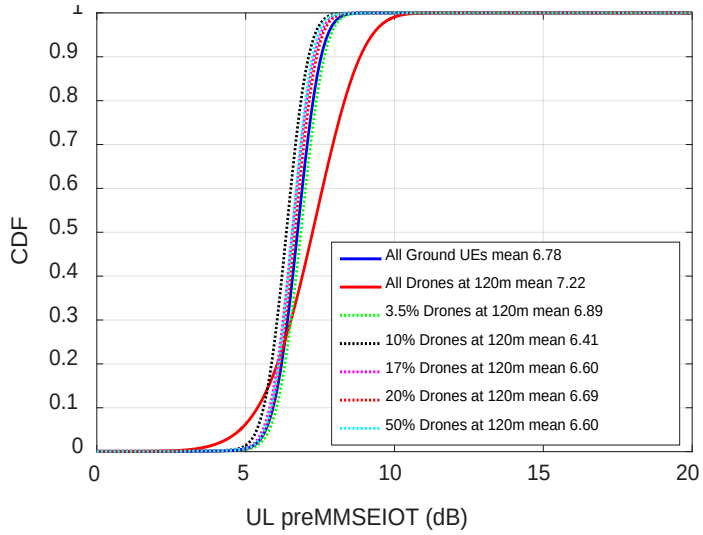

Figure 3-4 IoT distributions for Optimized OLPC

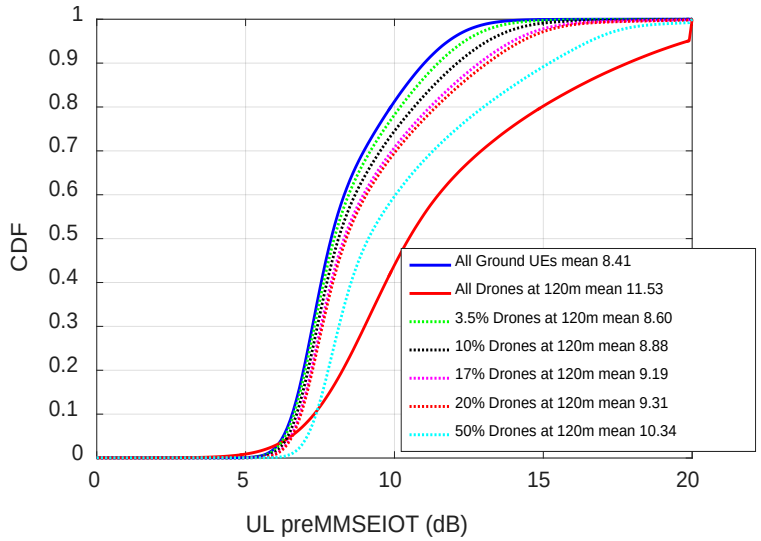

Figure 3-5 IoT distributions for CLPC

While managing interference is a key goal for uplink, it is not the whole objective. (Transmitting zero power does an excellent job of managing interference!) Next we look at the achieved throughputs for the same set of test cases.

Table 3-2 compiles the mean throughputs achieved across drone UEs at 120m and ground UEs separately. These means come from full distributions found in Appendix F.1.

We show the ground and drone UE throughputs separately to allow us to examine the impact of the presence of drones on the throughputs achieved by ground UEs, an important metric. Given the importance of this, the table highlights the reduction in mean throughput achieved on average by ground users relative to the all ground case (for the same power control settings) as a percentage in red text.

The overall conclusions from Table 3-2 are that power control optimizations can have a significant impact on throughput achieved in a network shared between ground and airborne UEs. It is somewhat surprising that even though Adaptive OLPC leverages knowledge of the difference between ground and airborne UEs, it does a relatively poor job of mitigating the degradation on ground users due to drones. The Optimized OLPC and the CLPC algorithms do comparatively well in these simulations. It is worth noting that 50% drone UEs in the network is viewed as a high proliferation of airborne UEs, and thus can be considered an extreme case.

Table 3-2 Mean throughputs per UE for different power control algorithms and for different splits between ground and drone UEs

Scenario	Mean UL Throughput (in Mbps)		
	Adaptive OLPC	Optimized OLPC	CLPC
All Ground UEs	0.37	0.48	0.44
All Drones at 120m	0.17	0.18	0.20
UEs+3.5% Drones (~1Drone/cell)	Ground: 0.32 (14%↓) Drone:0.56	Ground: 0.48 Drone: 0.32	Ground: 0.44 Drone: 0.31
UEs+17% Drones (~5Drones/cell)	Ground: 0.30 (19%↓) Drone:0.31	Ground: 0.44 (8%↓) Drone: 0.28	Ground: 0.41 (7%↓) Drone: 0.29
UEs+50% Drones (~15Drones/cell)	Ground: 0.24 (35%↓) Drone:0.23	Ground: 0.38 (20%↓) Drone: 0.22	Ground: 0.37 (16%↓) Drone: 0.24

3.4.2 Analysis of results – resource partitioning

While power control techniques were shown in the previous section to effectively control interference between ground and airborne UEs, full resource orthogonalization between these users can be another effective method to employ.

Here we present results of simulations the blocks of frequency resources (RBs) are dedicated to either ground or airborne UEs. Clearly, this method requires that the network is aware of the difference between UEs so their resources can be dedicated to the correct block. Further, given this simulation assumes the percentage of split follows the percentage of UEs of each category, and this split is uniform across all cells in the network, the results presented here are expected to be optimistic.

Given these assumptions, Table 3-3 presents the results of simulations where this resource partitioning was performed for the Optimized OLPC and CLPC power control cases. These results show resource partitioning effectively isolated the performance of each class of device, and prevented degradation of ground UEs, on average, as the percentage of airborne drone UEs increased.

Table 3-3 Mean throughputs per UE for different power control algorithms with frequency partitioning between ground and drone UEs

Scenario	Mean UL Throughput (in Mbps)	
	Opt. OLPC with RP	CLPC with RP
All Ground UEs	0.48	0.44
All Drones at 120 m	0.18	0.20
UEs+10% Drones (~3Drone/cell)	Ground: 0.48 Drone: 0.20	Ground: 0.45 Drone: 0.21
UEs+20% Drones (~6Drones/cell)	Ground: 0.48 Drone: 0.18	Ground:0.45 Drone: 0.19
UEs+50% Drones (~15Drone/cell)	Ground: 0.47 Drone: 0.18	Ground: 0.44 Drone: 0.20

3.5 Mobility simulations

Mobility simulations are performed to analyze handover performance and, in particular, to compare and contrast handover and link reliability between ground and airborne drone UEs.

These simulations are similar to the downlink and uplink simulations presented in the previous sections, except now UE motion is simulated. Each UE modeled starts at a randomly selected location in the network, and an angular bearing angle is selected randomly and uniformly. The UE then moves at the assigned speed in a straight line for the duration of the simulation.

NOTE: These simulations employ the concept of *wraparound* for computing signal powers in the network, and this concept also extends to UE position during motion. A UE that travels beyond the edge cell in the simulator appears immediately at the opposite side of the network and continues with the same speed and direction. There is no discontinuity in signal powers since the same wraparound is used for computing signal and interference powers.

Table 3-4 describes the parameters used to model the handover algorithm for these simulations. (Refer to Appendix C, *3GPP Technical Specification 36.331*).

Table 3-4 Parameters used to model the handover algorithm

Parameter	Value	Unit	Description
TimeToTrigger	160	ms	Time to trigger measurement report
A3Offset	2.0	dB	Offset between signal strength of serving and neighboring cells
MeasurementInterval	40	ms	Physical layer measurement interval
SamplesToAverage	5		Number of physical layer measurements averaged
L3RRMCoefficient	1		Filtering coefficient for layer 3 measurements
RMLInterval	2	s	Radio link monitoring interval
T310	1000	ms	Timer to trigger radio link failure recovery
HOPreparationDelay	50	ms	Handover preparation delay
HOExecutionDelay	40	ms	Handover execution delay
RSRPError	1.22	dB	Standard deviation of RSRP measurement error

The mobility simulations populate the network with 7 UEs per cell, on average. Simulations are performed with all UEs at ground, 50 m and 120 m altitude. Each of these are simulated with UE speeds of 0, 1.5, 3.0, 30, 60 and 120 km/h to gain an understanding of the handover performance dependency on speed.

3.5.1 Analysis of results

Here we evaluate the results of the handover (HO) simulations using six performance dimensions tabulated in Table 3-5, all are averages.

Table 3-5 HO simulations using six performance dimensions

KPI	Unit	Figure	Description
Handover rate	HO/UE/sec	Figure 3-6	Number of HOs over time
Radio Link Failure (RLF) rate	RLF/UE/sec	Figure 3-7	Number of RLFs over time
Time in handoff	%	Figure 3-8	Fraction of time a UE is in a HO procedure
Time in Qout	%	Figure 3-9	Fraction of time a UE is in Qout state
Handover interruptions	%	Figure 3-10	Percentage of HO procedures that start but fail

KPI	Unit	Figure	Description
Re-establishment interruptions	%	Figure 3-11	Percentage of HO re-establishment procedures that start but fail

Figure 3-6 shows the average number of handovers per UE per second.

As shown, drone UEs actually experience a smaller handover rate than ground UEs. Even though the amount of strong interference for drone UEs increases due to better radio propagation at higher elevations, the radio conditions are also more stable, which leads to reduced handover rate.

The handover rate for ground UEs is impacted by significant variation of received signal strength due to shadowing, which has standard deviation of 10 dB and decorrelation distance of 30 m.

At UE speed of 0 km/h, drone UEs experience slightly higher handover rates, due to static radio conditions for all UEs and larger impact of measurement errors on drone UEs.

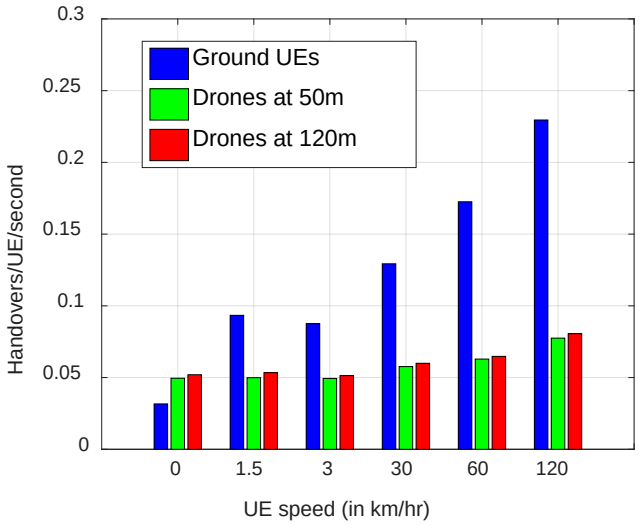

Figure 3-6 Handover rates

In LTE, radio link failure events are expected to be infrequent as shown in Figure 3-7. A relatively stable radio environment for drone UEs translates to virtually no RLF events during the system simulation run, even for drone UE speed of 120 km/h.

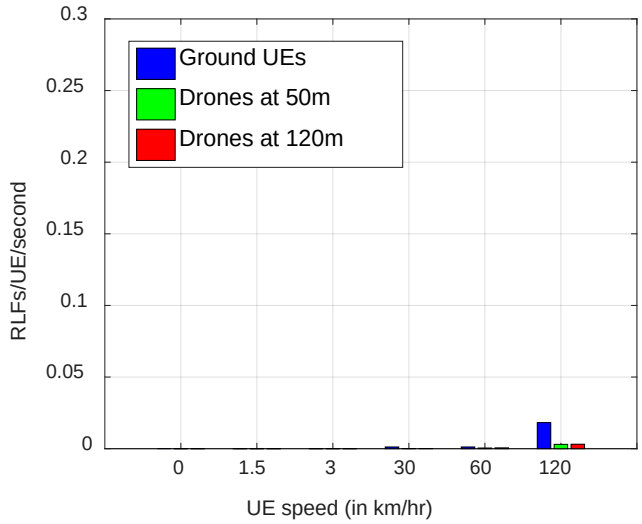

Figure 3-7 Radio link failure rates

In Figure 3-8 and Figure 3-9 we show the impact of handover of quality of service, measured by fraction of time communications with the UE is interrupted due to either handover events or radio link failures, respectively.

As seen in Figure 3-8, drone UEs experience significantly less time in handover than ground UEs for all speeds other than 0 km/h. The handover rates are UE speed of 0 km/h are very small and this speed is not of primary interest for drone UEs.

Figure 3-9 shows service interruption when signal quality drops below the Qout threshold, defined in 3GPP specs as SINR value of -8 dB. As shown, for all UE speeds whether they are on the ground or are drones at 50m and 120 m, these events are relatively infrequent.

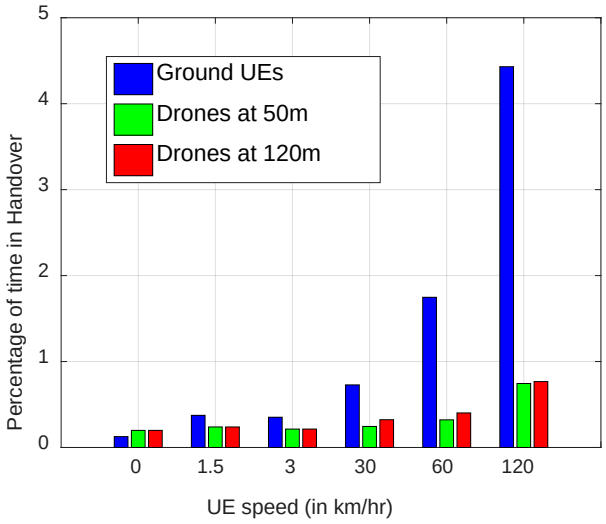

Figure 3-8 Fraction of time in handover

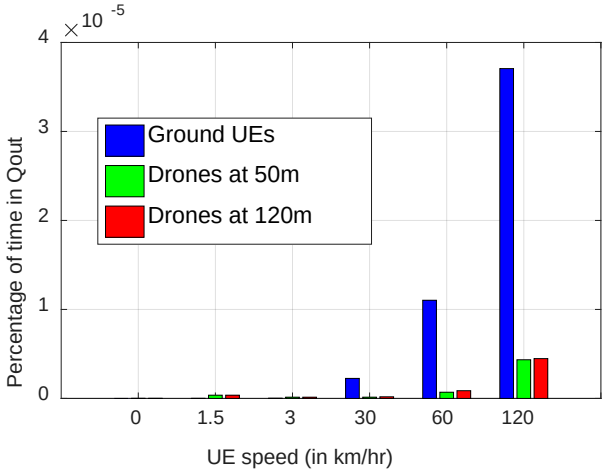

Figure 3-9 Fraction of time in Qout state

In Figure 3-10 and Figure 3-11, we show another view on the service interruption statistics.

Figure 3-10 illustrates the fraction of time service interruption was caused by handover.

Figure 3-11 illustrates the fraction of time service interruption was caused by radio link failure event and therefore triggered radio link reestablishment procedure.

As shown, there is a noticeable fraction of interruptions caused by radio link failure events only at high speeds.

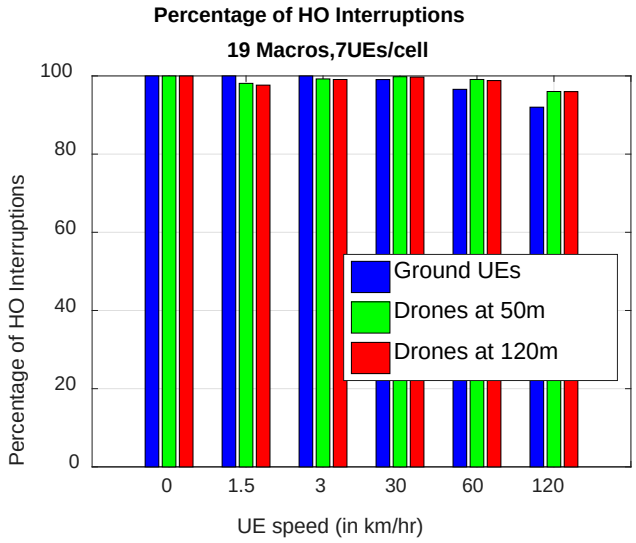

Figure 3-10 Likelihood of handover interruption

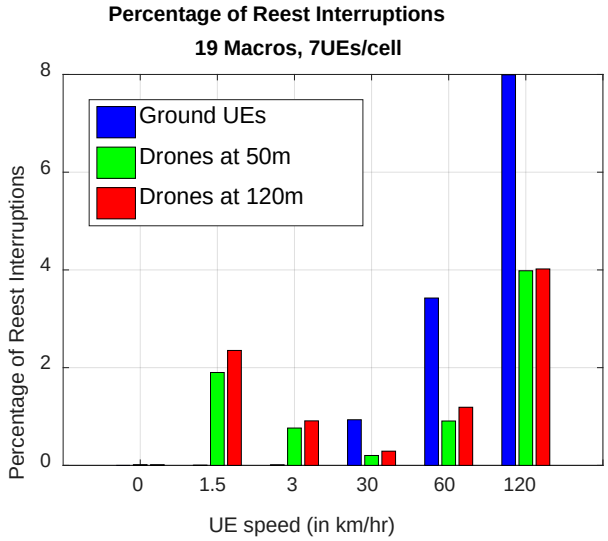

Figure 3-11 Likelihood of link re-establishment interruption

A Background

Small drones have many current or future applications, for example:

- Accident and crime scene investigation
- Aerial photography
- Agriculture inspection
- Construction inspection
- Crowd control
- Drug and gas detection
- Entertainment and movies
- Fire spotting
- Intelligence gathering
- Mapping and surveying
- Network tower inspection
- Newsgathering
- Payload delivery
- Pilot augmentation
- Pipeline/railroad inspection
- Power distribution tower inspection
- Search and rescue
- Security
- Small package delivery
- Traffic monitoring
- Wildlife and environment monitoring

This list of applications will expand over time as technology improves. To enhance utility and safety, the drones will be semi-autonomous and capable of performing certain tasks, including reacting to unforeseen challenges in their environment, using onboard sensing and processing. The drones will be in continuous communication with operations on the ground, providing status and telemetry and responding to mission directives as required. In addition, the drones may support direct connection from a ground based operator who can remotely take over control when required.

The communication requirements for UAS have strong overlap with requirements that have evolved over the past few decades in commercial wireless networks. They must scale to providing reliable and secure communications to millions of devices sharing scarce and valuable spectrum resources. An enormous investment has been made in developing the technologies required to meet the needs for commercial terrestrial wireless, and communication networks for UAS must leverage these technologies to be successful.

A network that meets UAS requirements will take time to fully implement and deploy, and we envision an evolution as the UAS scales that parallels and inFluences evolution in cellular network standards and implementation.

The remainder of this Appendix discusses general communication needs for UAS operations followed by a discussion of the current and planned capabilities of commercial wireless technologies in the context of UAS needs.

A.1 UAS communication needs

The list below outlines the general needs for UAS communication links but does not suggest specific requirements necessary to meet regulatory needs addressing safety and integration into National Airspace System (NAS).

Telemetry

This refers to data from the unmanned aerial vehicle (UAV) reporting various status messages and sensor results. Examples are position, altitude, velocity/airspeed, attitude and heading, fuel/power status, communication link quality, etc. These data messages could be used for mission status and planning, data logging, coordination, and situation awareness for ground stations. Some data messages are streamed at a fixed rate, and other messages are conditional alerts (such as low battery indication). The data bandwidth requirements are relatively low (10s of kilobits per second). Reliability and latency requirements depend on the use case.

Real-time video

Many applications benefit from, or require, real-time video feeds from onboard cameras. These videos can be used to augment or provide situation awareness for piloting and for real-time mission analysis and adjustments. Video bandwidth depends on resolution and frame rate, but 1-10 megabit per second is typical for high quality video. If the video stream is used for flight navigation and situation awareness, sub-second latency is typically needed.

Command and control

In addition to data streams from the UAV, two-way links that enable sending commands to the drones and receiving responses are required. This datalink supports messages such as navigation commands, waypoint entry, configuration adjustments, information requests and safety commands. Like telemetry, since the data traffic consists of small data packets, the overall communication bandwidth per UAV is small (<10 kilobits per second). However, if command and control is used in conjunction with real-time video to make piloting decision, then sub-second latency is typically needed.

Application data transfer

The various applications and use cases for commercial UAS will require application specific data transfers such as sensor measurements and images collected. Application updates and configurations must also be supported, and the ability to use the existing datalink for such transactions will be required.

Vehicle to vehicle

UAS use cases that employ multiple drones in close proximity can benefit from knowledge of neighbors' presence and position. This knowledge can be used simply for avoidance, or in some cases for cooperation between drones. Depending on the specifics, the links that facilitate this information transfer could be direct (from vehicle to vehicle) or routed through a control station.

NAS system integration

Coexistence of UAS in the NAS with piloted vehicles requires the capability to communicate and coordinate with air traffic control (ATC) operations. This integration must ensure the performance and security of safety critical communications with the UAS, and the impact on ATC communication systems must be acceptable.

Lawful intercept

A network in communication with UAS must support a mechanism for intercept by authorized parties in the event of an emergency. This intercept could be simply for status information, for transmission of exclusion zones, or for forced landing in extreme cases.

A.2 Commercial mobile technologies

This section outlines key features of commercial mobile networks (Section A.2.1) and the devices/radios/chipsets that operate in these networks (Section A.2.2) and relates these features to the needs of UAS. Then, a discussion of a few of the main areas of near-term evolution is given in Section A.2.3.

A.2.1 Features and capabilities of commercial mobile networks

Over the past few decades, commercial mobile networks have evolved at a rapid pace due to the competitive market for providing voice and data connectivity. There has been a significant investment by wireless operators, equipment vendors, and technology developers to engineer robust and high-performance networks and to deploy, operate, maintain and evolve these networks. Some of the key capabilities that have emerged and refined are described here.

Coverage

Combining the networks of the major service providers, coverage has now reached the point where it is essentially ubiquitous in areas where there is high population density. In high density areas, coverage is provided in most indoor locations as well. Since the need for connectivity is strong for travelers, coverage is also particularly strong along on interstate highways and other major roads.

It is worth noting that providing strong coverage to a few mobile devices in a network is not a particularly difficult problem that was achieved first by military systems during WWII (e.g., SCR-299). However, ubiquitous coverage for a large number of mobile devices requiring simultaneous service in limited spectral resources is a substantial challenge. First, a network provider must acquire sites for housing cell site equipment and mounting antennas where there is sufficient electricity and temperature control to run the equipment. These sites must have a connection to a sufficiently high-bandwidth backhaul network to connect with wireline voice and data networks. Further, there are typically local regulations on the height and appearance of antenna arrays that must be followed. (Refer to Appendix C, *Tower and Antenna Siting.*)

Due to the presence of multiple base stations that inevitably transmit toward each other, and due to the reality of terrain features (hills, valleys, trees, buildings) which cause complex signal propagation variations, transmit power and antenna pointing optimizations are required to manage coverage and interference. These optimizations are critical to the overall network performance. Finally, the network is not static. Ever increasing market demands for higher data rates and improved service quality means base stations are continuously updated, added, and adjusted and this is done without interrupting service to customers.

These coverage challenges relate directly to UAS since the safety of operation depends on network availability. Further, UAS required coverage extends from the ground (which is still needed for takeoff and landing) to operation altitudes.

Multiple access

Simultaneous service to multiple mobile devices (or multiple access) is strongly related to coverage since the channel resource usage and interference generated by the competing devices impact the coverage provided. There are many techniques current commercial networks employ to efficiently manage multiple devices, and a few of the main techniques are mentioned here. First, idle devices (ones not actively transmitting) need to stay in contact with the network so they can be quickly reached when needed. And this needs to be done with minimal overhead on the network and at low power consumption in the device. Years of evolution have resulted in highly optimized access and paging designs to manage idle-mode operation.

Since the devices requiring service are at different locations in the network and inevitably have significantly different signal quality from the base station(s), methods for adjusting transmissions based on the instantaneous signal available are required. Matching the transmissions to the needs of the device is critical to managing interference. Techniques for this include signal quality feedback, dynamic transmit power control, and dynamic data rate adaptation. In addition, dynamic channel scheduling algorithms are used that allocate channels (split by time, frequency, code, and space) to the multiple competing devices in the network. (Refer to Appendix C, *Comparing Different LTE Scheduling Schemes.*)

For UAS, these multiple access technologies are critical to managing the network resources as the number of drones increase.

Mobility

A key feature of a mobile network with multiple base stations is the ability to handoff an active connection as the device moves between the coverage areas of different base stations. Since early networks focused on voice, it was necessary to achieve handoffs without being perceptible to the user during a phone call. This requires the mobile device to constantly monitor the availability and signal quality of candidate neighboring base stations, and to quickly handoff the channel between base stations when the handoff decision is made. On the network side, the data/voice traffic must be seamlessly stitched together when a hand off occurs.[1,2]

This type of mobility is critical to networks for UAS to enable continuous connections to be available as drones move throughput the network. Note that LTE was designed to support operation and handoff at speeds up to 450 km/h for use on existing and future high speed trains.

[1] It is worth noting that some systems have used so-called s*oft-handoff* where a device is simultaneously connected and transmitting to two base stations during the handoff sequence.

[2] In addition to handing off connections between base stations operated by the same network provider, the commercial wireless industry has developed technical approaches and business agreements that allow roaming between providers. This enhances coverage available to a user/device since it can seamlessly interoperate between networks with different coverage footprints.

Security

Security has been a required feature in commercial mobile networks since the digital revolution for ensuring authorized access to service, to protect user communications from eavesdropping, and to prevent unauthorized access to the network infrastructure that could result in service outage. Security protocols involve user/device authentication, key generation, exchange and management, mutual authentication, encryption and decryption. The security mechanisms developed and adopted in the wireless network standards bodies have benefitted from intense scrutiny by wireless professionals as well as by security experts in industry and academia. (Refer to Appendix C, *LTE Security*.) And clearly strong security is required for UAS to protect the integrity of the network, the data and information generated, and the UAV command and control.

QoS

Quality of Service is the term used for the techniques that enable differentiated service level for different users, channels, and/or applications. Not only can messages be prioritized, but channels (called *bearers* in LTE) can be established depending on the latency requirements for the application. For example, voice-over-IP traffic does not require a very high data-rate, but the application is sensitive to delay and gaps in packet delivery. QoS mechanisms allow the network to be informed of the application quality requirements, and to adjust data delivery methods to achieve those requirements. For more information, the top-level QoS design for LTE is described in *3GPP Technical Specification 23.401 v12.5.0,* Section 4.7 (see Appendix C).

For UAS, QoS capabilities can be useful for the network to manage different priorities for connections. As an example, a UAV requiring assistance from a ground operator to perform a safe landing has a higher priority than a UAV that has already landed. QoS features that allow the network to adjust service quality based on dynamic connection priorities enhance the overall safety of the UAS.

A.2.2 Features and capabilities of commercial mobile devices

Along with the evolution of mobile networks outlined in the previous sections of this paper, the user equipment (i.e., devices and the chipsets and other technologies embedded in this equipment) is constantly evolving and improving at a rapid pace.

Here is a summary of some of the key features of mobile broadband devices:

Low power

Since battery life has always been a principal driver in the market, techniques for minimizing energy consumption across all features in a mobile device are extremely important and a major focus of investment and effort by QTI. and other suppliers. Indeed, the industry expects power efficiency will be continuously enhanced with each product release. The improved power efficiency is either used to lengthen battery life between charges, or to enable additional features and capabilities within the product's energy budget. This is important for drones to lengthen the operational time of the vehicle between charges, especially as the onboard computational and communication load for sophisticated sensor processing and autonomy increases.

Multimedia

More recently, large screen smartphones with video cameras and high-bandwidth connections to the internet have generated a requirement for high-performance multimedia capabilities on the device. Today, the latest mobile broadband devices handle real-time video encoding and decoding at up to high-definition (HD) resolution and frame rates enabling applications such as HD video streaming and real-time, 2-way video telephony. At the end of 2013, devices supporting ultra HD video (i.e., 4K video) became available (used first for external displays with 4K smartphone touch displays expected to arrive in the first half of 2015) High-performance graphics processing cores are common as well enabling high-resolution 3D graphics and computer vision.

Security and encryption

The need to secure both voice and data transmissions in modern networks have led to security and encryption as standard features in wireless chipset products. Thus, optimized implementations of encryption and decryption are available as well as secure cryptographic key storage and management on the device. As an example, most large banks now provide smartphone apps to their customers that allow account management, transactions, and check scan/deposit from the device.

Integration

Space limitations for mobile devices you can carry in your pocket have led to a high level of integration of features into as few chips as possible. Modern chips and SoC (system on chip) architectures often include essentially all of the necessary functions for a smartphone other than RF (antenna connectors, filters, and mixers) and power management. This level of integration is intended to make it easier and more economical for a smartphone designer to offer a full-featured product.

Sensor processing

Smartphones on the market today have the following integrated sensing capabilities beyond the radio transceivers:

- 3-axis accelerometer
- 3-axis gyroscope
- 3-axis magnetometer/compass
- Pressure sensor/barometer
- Ambient light sensor
- Proximity sensor
- Audio microphone
- Camera (multiple)

Location features

The ability for a mobile device to locate itself has been evolving over the past decade, and current devices have sophisticated circuitry and software algorithms for providing location and related features.

For example, QTI provides chips today that integrate a global navigation satellite services (GNSS) receiver that routinely tracks 20+ satellite signals (from multiple constellations) for sub-2 meter position accuracy in open sky conditions. Aiding features are supported in some products (such as local-area and wide-area differential GPS) which remove known errors during processing further improving accuracy.

Further techniques that use ranging signals transmitted by LTE base stations for precise location are available (called observed time difference of arrival or OTDOA). In addition, techniques that fuse satellite and OTDOA based information with inertial sensors also integrated in the product can provide further improvements in accuracy and sample rates. On top of these location features are services such as geofencing which provide alerts when the device enters or exits pre-defined boundaries in space.

A.2.3 Evolution of mobile network technology

To keep pace with demand, the process of developing enhancements to mobile technologies and implementing those technologies in mobile networks continues at a rapid pace. Today, many new technologies are in the pipeline, and here we focus on three primary categories: link enhancements, small cell deployments, and heterogeneous networks, and discuss their relevance to UAS.

Link enhancements

Larger amounts of spectrum are being allocated for commercial mobile networks and new technologies and standards are currently under development to further optimize the use of this spectrum.

First, interference cancellation techniques help receivers to not only reduce noise from neighboring users' transmissions but effectively estimate and erase them from the incoming signal before demodulation. (Refer to Appendix C, *Interference Cancellation for Cellular Systems*.)

Second, enhanced multi-antenna methods such as multiple-input and multiple-output (MIMO) and beamforming are being designed for use in wide-bandwidth channels that can enable effectively pointing of the signals to increase the intended user SNR while reducing interference to other spatially separated users. (Refer to Appendix C, *Fundamentals of Wireless Communication.*) A new aspect of this optimization is being designed that enables dynamic coordination between base stations as the users they serve move in the network.

Finally, because available spectrum is sometimes in non-contiguous blocks, techniques that allow the aggregation of spectrum in different bands into a single effective channel can significantly increase peak data capacity and speeds. (Refer to Appendix C, *Carrier Aggregation Explained.*) This technique is known as carrier aggregation. It allows wireless operators to bond spectrum in different bands to create channels that are up to 100 MHz wide, leading to very high average and peak data rates. Currently, devices with chips supplied by QTI already support 40 MHz aggregation in the downlink (i.e., base-to-mobile), and further increases are planned over the next two years.

Link enhancements create benefits for all uses (throughput per device, number of devices supported, coverage, etc.). But because signals from ground-air and air-ground propagate further than ground-ground signals, interference can be larger for aviation use relative to terrestrial use. As a result, interference management from cancellation and spatial processing is expected to be particularly beneficial for UAS.

Small cell deployments

Ubiquitous coverage indoors and outdoors has always been a goal for commercial mobile networks, but it is well known that this is a significant challenge. Terrain variations affect signal propagation, penetration losses can be significant for indoor coverage, and covering large areas is costly.

A promising approach is being developed that allows deployment of base stations with very different coverage areas in the same network. Traditional high power base stations deployed on towers, called macro cells, have a coverage area of several kilometers. But, macro cells can be augmented with deployment of so-called small cells, which use much less power and do not need to be deployed on a tower. These small cells include so-called femto cells and pico cells. These cells can cover a home and its close surroundings. With a dense enough deployment of small cells in a residential area, an entire neighborhood can be covered, for example. These small cells can provide much better service quality to a user while limiting the impact of this user on the larger network due to the lower transmission powers required to maintain a connection. (Refer to Appendix C, *Femtocells: Past, Present, and Future.*) The macro cells then can be focused on delivering service to a reduced set of users who are not in range of these smaller cells. Small cells cost much less than macro cells and, because they do not need to be deployed on towers, are not as limited by zoning laws. Small cells can be deployed in areas where cellular coverage is insufficient, increasing the uniformity of coverage in the network.

Integration of small cells into a cellular network comes with significant technical challenges. First, managing interference becomes much more difficult when there is a variety of transmit powers and coverage areas for different base stations and especially when the cells overlap – a common occurrence in small cell deployments. To address this challenge, techniques (called SON, for self-optimizing networks) are under development that enable the network to adjust parameters automatically and dynamically after deployment to adapt to the existing interference. (Refer to Appendix C, *Qualcomm® Small Cells.*) In addition, the existence of more base stations can result in a much higher rate of handoff for a user moving through the network. This can over-burden the network and reduce link quality in some cases. Thus, special techniques for controlling handoffs that are aware of the small cells are required and are under development.

Another goal for small cells is to facilitate local coverage improvement by enabling simple deployment and activation of a small base station or set of small base stations. These would automatically integrate into the larger wireless network, or in an isolated area, could simply provide local wireless connectivity to the wired network (on a remote farm, for example). This would enable a UAV to operate in these locations using the same radios and protocols as existing cellular networks use today.

For UAS, the ability to deploy small cells easily to enhance coverage and capacity will enable safety and performance improvements in selected geographical areas. Examples include takeoff and landing locations, areas of high UAV density, and specific mission focus areas. These small cell deployments could be semi-permanent, or could be temporary depending on mission needs.

Heterogeneous networks

Heterogeneous networks not only utilize cells of different sizes and coverage areas, as mentioned in the previous section, but also are comprised of a range of technology types available to users -- from different cellular standards to WiFi over unlicensed frequency bands. Techniques are under development to allow a device to take advantage of these heterogeneous networks to optimize link availability, performance, and service cost. Going beyond simply enabling connectivity from the disparate networks, these techniques are designed to coordinate service such that an existing connection can be handed off to a different network while maintaining a continuous connection. The next generation standard will also support network coordination techniques such as enhanced inter-cell interference coordination (eICIC) which promise to offer a substantial performance boost for receivers that support these features.

Figure A-1 illustrates the deployment model for future mobile networks that integrate both small cells and heterogeneous networks.

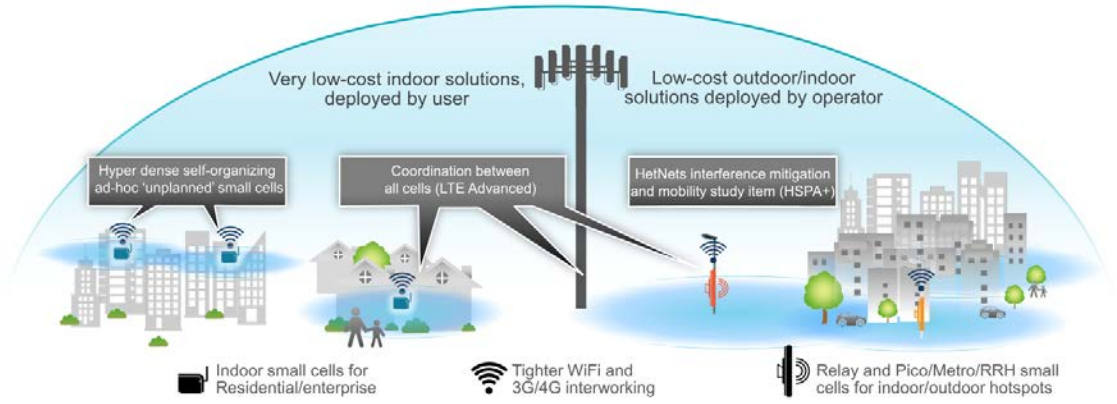

Figure A-1 Modern Network Deployment Model – Small cells and heterogeneous networks

B Acronyms, Abbreviations, and Terms

Table B-1 provides definitions for the acronyms, abbreviations, and terms used in this document.

Table B-1 Acronyms, abbreviations, and terms

Term	Definition
3GPP	3rd Generation Partnership Project
ATC	Air traffic control
AWS	Advanced Wireless Service
BW	Bandwidth
CLPC	Closed loop power control
DL	Downlink
eICIC	Enhanced inter-cell interference coordination
FAA	Federal Aviation Administration
GNSS	Global navigation satellite services
HD	High-definition
HO	Handover
IoT	Interference to thermal
IPerf	Internet performance
LTE	Long-term evolution
MIMO	Multiple-input and multiple-output
NAS	National Airspace System
OLPC	Open loop power control
OTDOA	Observed time difference of arrival
PCI	Physical cell indicator
PCS	Personal Communications Service
QoS	Quality of service
RACH	Random access channel
RB	Resource block
RC	Radio-controlled
RF	Radio frequency
RLF	Radio link failure
RS	Reference signal
RSRP	Reference signal received power
RSRQ	Reference signal received quality
RSSI	Received signal strength indicator

Term	Definition
SD card	Secure digital card
SINR	Signal-to-interference plus noise ratio
SNR	Signal to noise ratio
SoC	System on chip
SON	Self-optimizing networks
TPL	Total path loss
UAS	Unmanned aircraft system
UAV	Unmanned aerial vehicle
UDP	User Datagram Protocol
UE	User equipment
UL	Uplink

C References

The references listed in Table C-1 provide additional information about topics discussed in this document.

Table C-1 References

Title, Author	Location/Source
Qualcomm Technologies, Inc.	
Hetnets, An overview of heterogeneous network features in LTE	http://www.qualcomm.com/research/projects/lte-advanced/hetnets
LTE Direct, An overview of LTE-D with linked resources.	http://www.qualcomm.com/research/projects/lte-direct
Small Cells, An overview of small cells and self-organizing network techniques	http://www.qualcomm.com/research/projects/smallcells
Wireless Networks Information site at Qualcomm.com	http://www.qualcomm.com/solutions/wireless-networks/technologies/
External	
3GPP Technical Specification 23.203 v13.0.1	http://www.3gpp.org/DynaReport/23-series.htm
3GPP Technical Specification 23.401 v12.5.0	http://www.3gpp.org/DynaReport/23-series.htm
3GPP Technical Specification 36.213 v13.0.0, Section 5.1.1.1, for PUSCH power control	http://www.3gpp.org/DynaReport/36-series.htm
3GPP Technical Specification 36.814 v9.0.0, Appendix A2 for system simulations	http://www.3gpp.org/DynaReport/36-series.htm
3GPP Technical Specification 36.331 v8.2.0	http://www.3gpp.org/DynaReport/36-series.htm
4G Americas White Papers, A resource for information on next-generation networks	http://www.4gamericas.org
Carrier Aggregation Explained, 3GPP	http://www.3gpp.org/technologies/keywords-acronyms/101-carrier-aggregation-explained
Comparing Different LTE Scheduling Schemes, S.A. AlQahtani and M Alahssany, Proc. 9th International Wireless Communications and Mobile Computing Conference, 2013	http://ieeexplore.ieee.org/stamp/stamp.jsp?arnumber=6583570
FAA Pilots Handbook: Airspace, FAA	https://www.faa.gov/regulations_policies/handbooks_manuals/aviation/pilot_handbook/media/PHAK%20-%20Chapter%2014.pdf
Femtocells: Past, Present, and Future, J.G. Andrews, J. Claussen, M. Dohler, S. Rangan, M. C. Reed, IEEE Journal on Selected Areas in Communications, Vol. 30, No. 3, April 2012	http://ieeexplore.ieee.org/stamp/stamp.jsp?arnumber=6171992
Forsk Atoll	http://www.forsk.com/atoll/
Fundamentals of Wireless Communication, David Tse and Pramod Viswanath	Cambridge University Press, 2005

Title, Author	Location/Source
Integration of Civil Unmanned Aircraft Systems (UAS) in the National Airspace System (NAS) Roadmap, First Edition, Federal Aviation Administration, November 2013	http://www.faa.gov/about/initiatives/uas/media/UAS_Roadmap_2013.pdf
Interference Cancellation for Cellular Systems: A Contemporary Overview, Jeffrey G. Andrews, IEEE Wireless Communications, April 2005	http://ieeexplore.ieee.org/document/1421925/
LTE Security, D. Forsberg, G. Horn, W-D Moeller, V Niemi	John Wiley and Sons Ltd., 2013
National Broadband Map, NTIA in collaboration with the FCC. Data as of June 30, 2013	http://www.broadbandmap.gov/summarize/nationwide
Tower and Antenna Siting, A guide from the FCC	http://www.fcc.gov/encyclopedia/tower-and-antenna-siting
Unmanned Aircraft Systems (UAS) Comprehensive Plan, The Joint Planning and Development Office (JPDO), September 2013	http://www.jpdo.gov/library/UAS_Comprehensive_Plan.pdf
Verizon Annual Report, 2013	http://www.verizon.com/investor/quicklink.htm
Wireless Quickfacts, CTIA	http://www.ctia.org/your-wireless-life/how-wireless-works/wireless-quick-facts

D Estimating UL Received Power from UE Logs

To validate the accuracy of using downlink path loss to estimate uplink received power, lab tests were performed using an LTE small cell that can measure received energy directly. Validating in lab increases confidence this method can be employed for estimating received power in field testing.

First, the setup shown in Figure D-1 is used to test this method in a cabled up scenario (as a baseline). Downlink RF is passed through a variable attenuator, which is used to sweep through different path loss conditions. The small cell is configured with 2x2 MIMO and UE has a single transmit antenna port on the uplink. The splitter/combiner combination is used so both the receive antennas are subject to identical RF conditions. The tethered laptop to the UE is used to collect UE logs and initiate uplink and downlink traffic over the LTE connection.

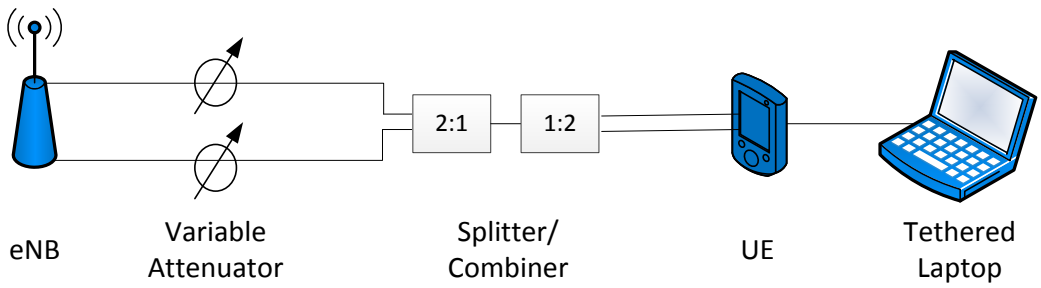

Figure D-1 Cabled setup

As shown in Figure D-2, a second over-the-air setup, similar to the cabled setup in Figure D-1, was used to perform the same test in over-the-air conditions.

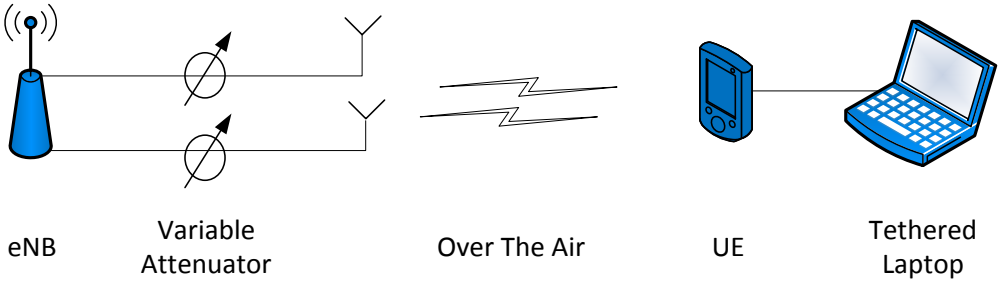

Figure D-2 Over-the-air setup

UE logs are used to measure DL reference signal received power (RSRP), DL received signal strength indicator (RSSI), and UE transmit power. Logs from the small cell are used to measure the physical layer uplink RSSI. Since there is only one UE in this setup, the RSSI measured is equal to the received power from transmissions from this UE. A full buffer UDP traffic stream is generated both on the uplink and downlink. All the resource block allocations on downlink and uplink are assigned to this UE.

Path loss is calculated as: PL = configured RS power - DL measured RSRP

Measured uplink RSSI = Rx RSSI from small cell logs

Predicted RSSI = UE Tx power – PL

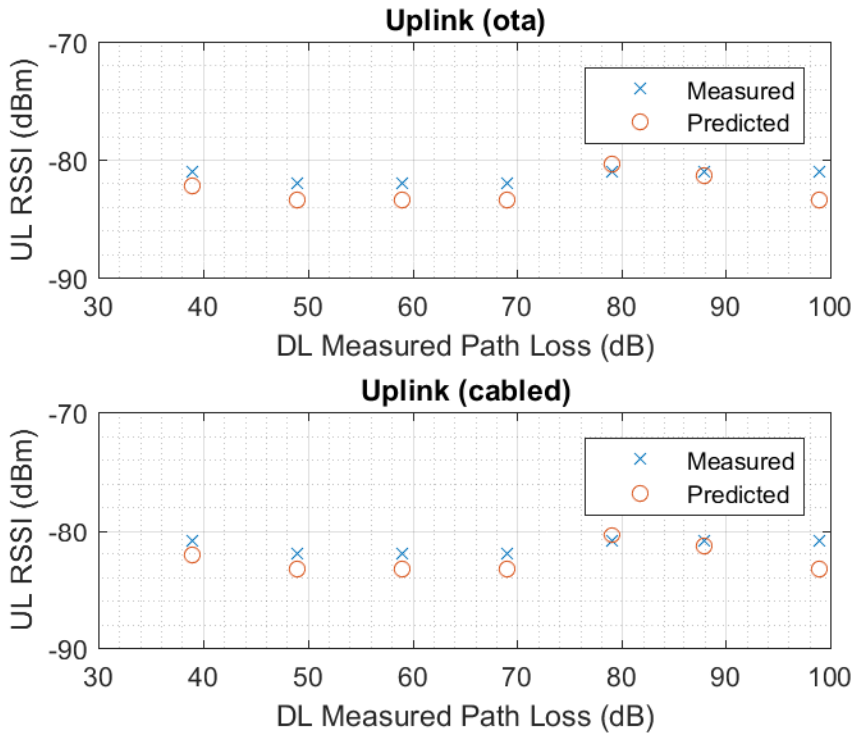

Figure D-3 DL measured path loss

In Figure D-3 cross points represent the measured uplink RSSI at the base station at the PHY layer. The circled points represent the predicted RSSI from the UE transmit power values from the UE logs based on the formula described above. The plot shows the measured and predicted values are generally within on 1 dB across this range of path loss values. This gives us further confidence this estimation method can be used for analysis of field data.

E Antenna Patterns

E.1 Drone patterns

The antenna patterns of the drone/antenna combination were measured in a testing chamber according to the *CTIA OTA Performance Test Plan* procedures. Free space measurements were conducted for Bands PCS, AWS and 700 MHz measuring,

- TRP and EIRP vs. elevation/azimuth
- TIS and EIX (Rx sensitivity) vs. elevation/azimuth
- EIRP and EIS sweeps across full frequency ranges

These measurements were conducted while the drone and its electronics were fully operational and active to account for potential for local EMI influencing the patterns.

The coordinate frame for this testing is

- x-axis: out the vehicle nose
- y-axis: out the left side of the vehicle, at a 90 degree angle from the x-axis
- z-axis: out the top of the vehicle, at 90 degree angles from both the x and y-axes

Elevation is defined here as the angle of direction down from the z axis. Azimuth is the horizontal plane rotation about the z-axis starting aligned with the x-axis.

Figure E-1 shows the resulting antenna patterns.

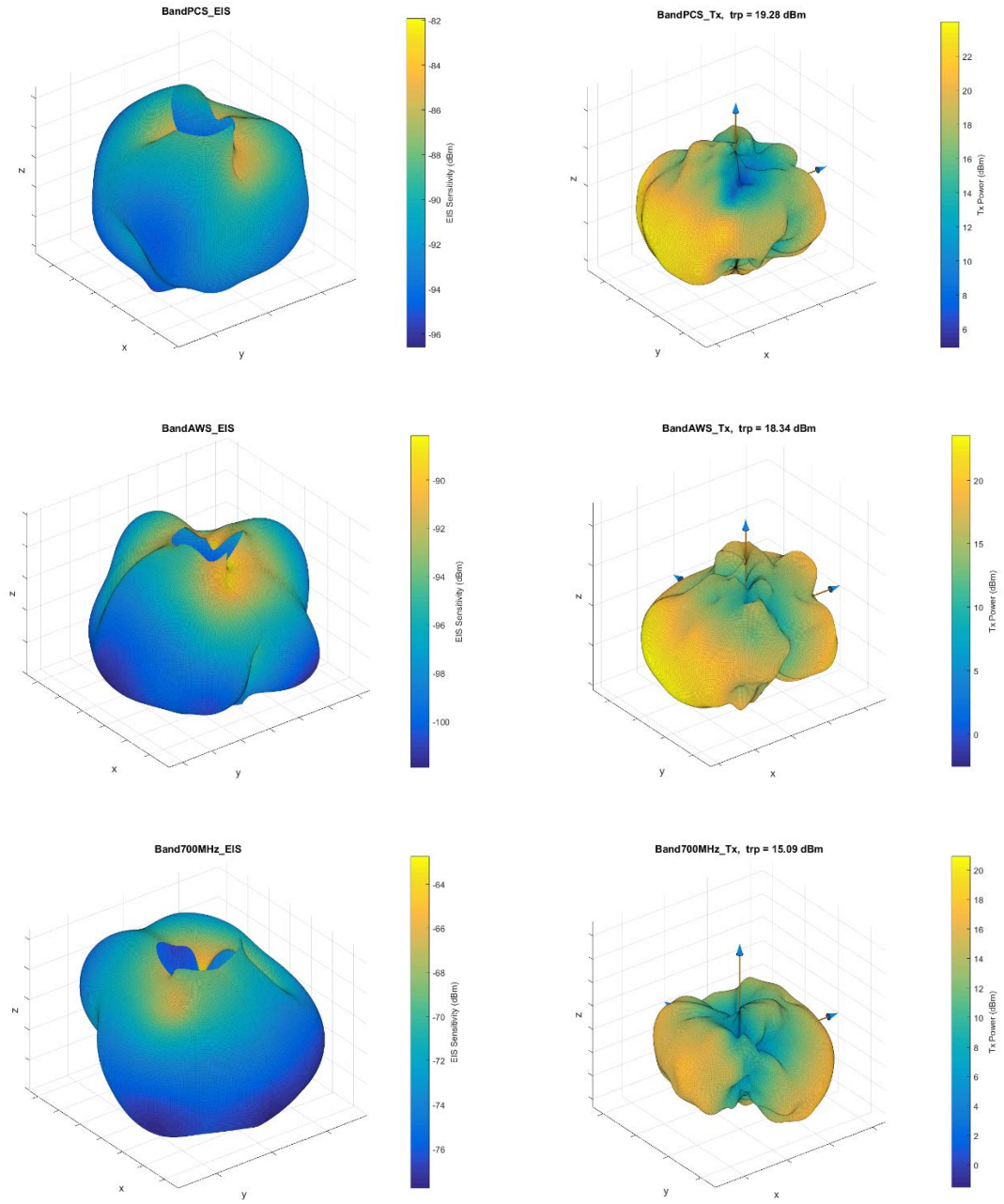

Figure E-1 Drone antenna patterns

E.2 Base station cell antenna pattern

The base station antenna patterns used in this study are represented here. There are too many antennae used (>100 including a unique pattern for each value of electronic tilt used), so one typical antenna pattern is given.

The coordinate frame for modeling the patterns is

- x-axis: out the antenna boresight
- y-axis: out the left side of the antenna, at a 90 degree angle from the x-axis
- z-axis: out the top of the antenna, at 90 degree angles from both the x and y-axes

Elevation is defined here as the angle of direction below the horizontal plane (the plane that contains the x and y-axes, note this is positive down). Azimuth is the horizontal plane rotation about the z-axis starting aligned with the x-axis.

Figure E-2 provides the 3D pattern of a typical sectored antenna.

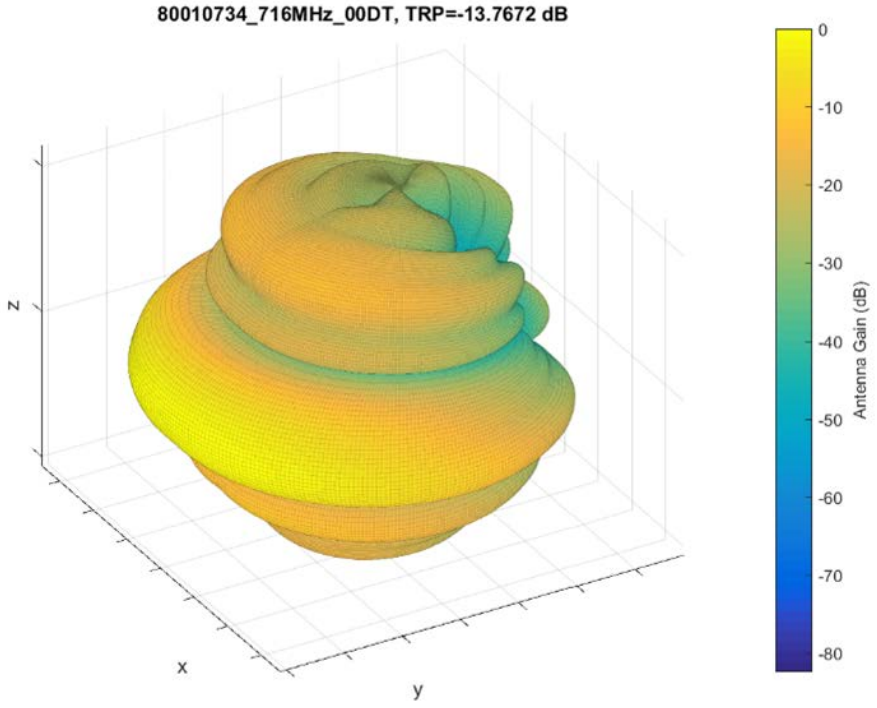

Figure E-2 An example base station cell antenna pattern

F Additional Plots

F.1 Simulated uplink throughput distributions

Figure F-1 through Figure F-5 show uplink throughput distributions.

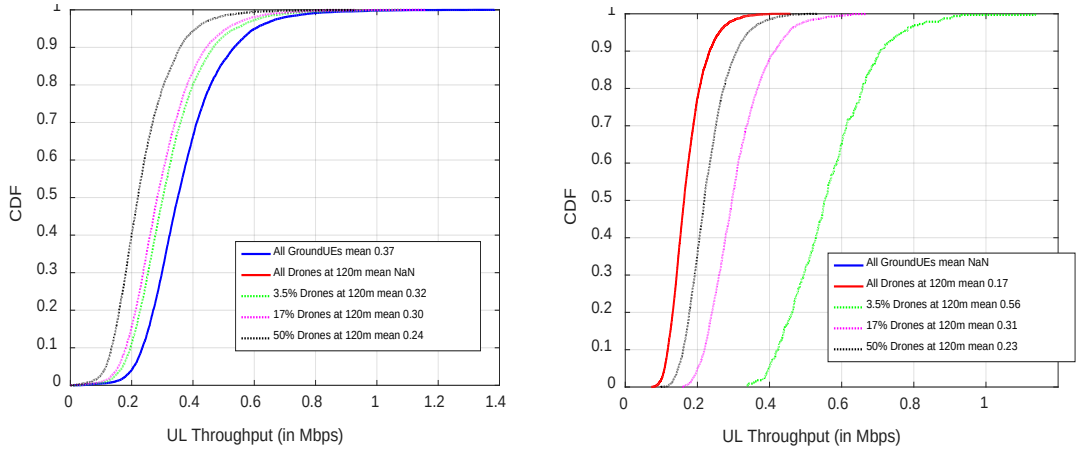

Figure F-1 Uplink throughput distributions for Adaptive OLPC

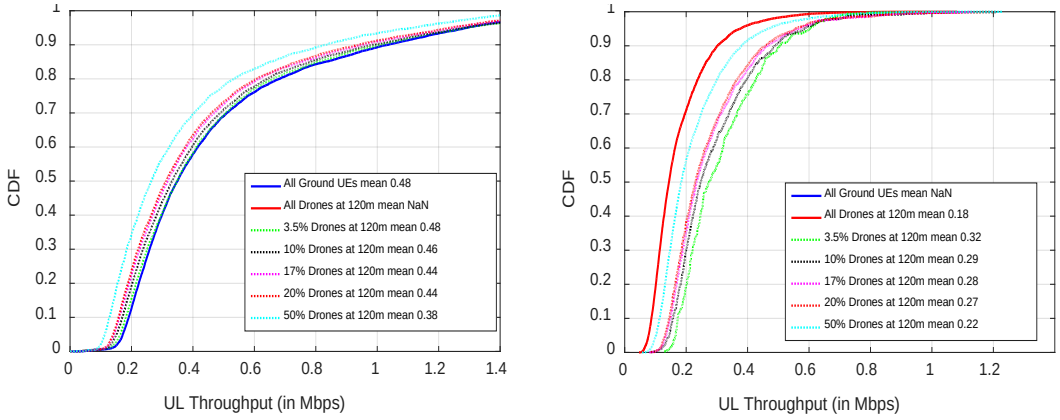

Figure F-2 Uplink throughput distributions for Optimized OLPC

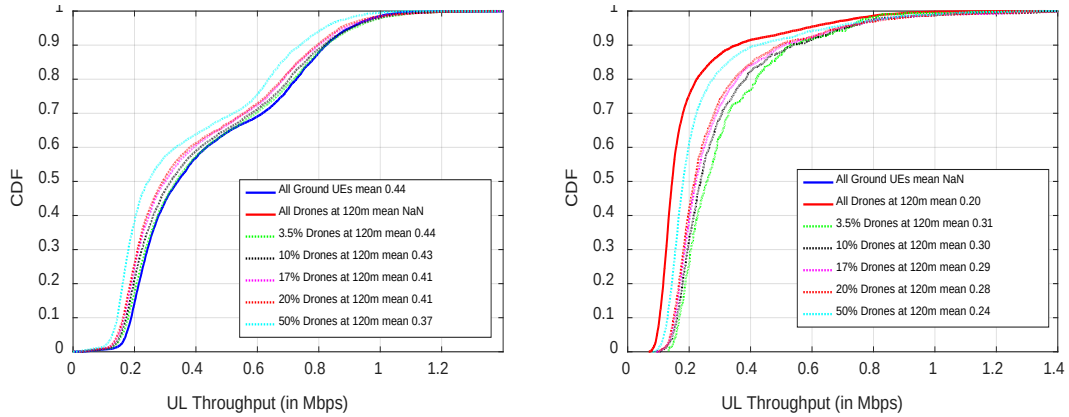

Figure F-3 Uplink throughput distributions for CLPC

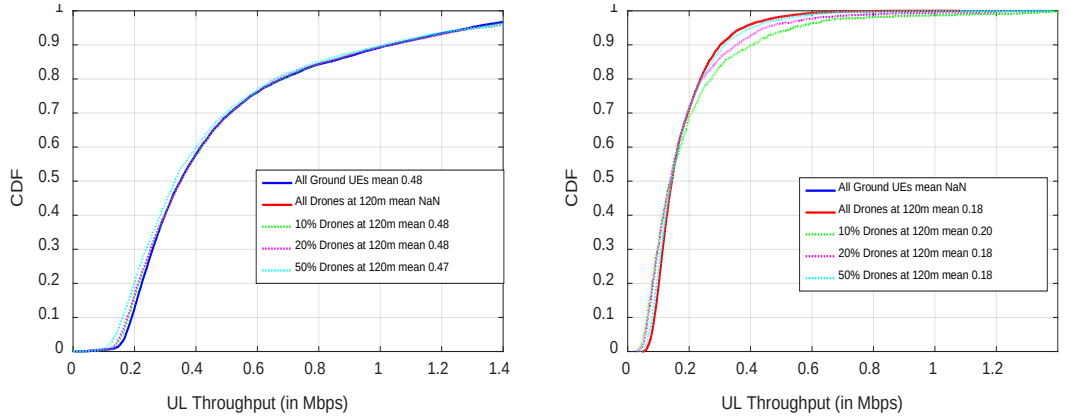

Figure F-4 Uplink throughput distributions for Optimized OLPC with resource partitioning

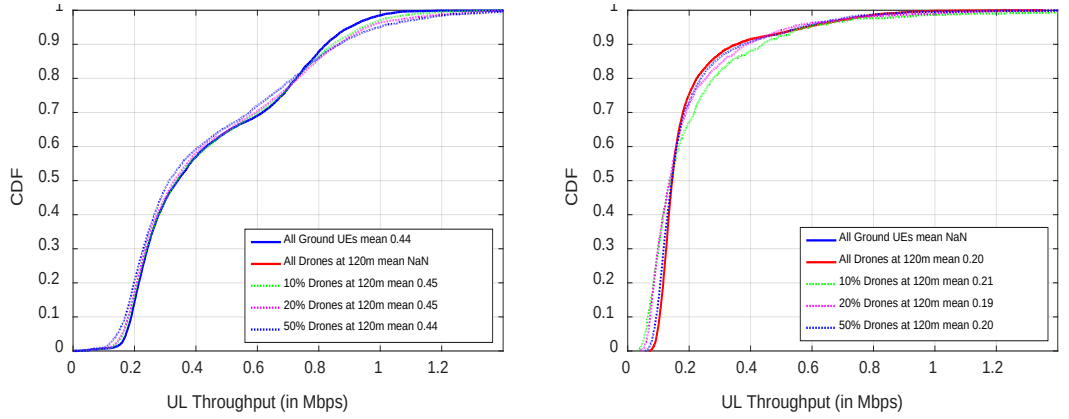

Figure F-5 Uplink throughput distributions for CLPC with resource partitioning